



Trinity College Dublin
Coláiste na Tríonóide, Baile Átha Cliath
[The University of Dublin](#)

School of Physics

Athermalisation of semiconductor lasers operating at 1.3 and 1.5 microns

Michael Glennon

March 20, 2021

A Final Year Project submitted in partial fulfilment
of the requirements for the degree of
B.A. Physics

Declaration

I hereby declare that this Final Year Project is entirely my own work and that it has not been submitted as an exercise for a degree at this or any other university.

I have read and I understand the plagiarism provisions in the General Regulations of the University Calendar for the current year, found at <http://www.tcd.ie/calendar>.

I have also completed the Online Tutorial on avoiding plagiarism 'Ready Steady Write', located at <http://tcd-ie.libguides.com/plagiarism/ready-steady-write>.

Signed: _____

Date: _____

Abstract

The tunable laser diode is a key component in optical communications technology. Its ability to operate at a precise and consistent wavelength has enabled the development of infrastructure that can allow many lines of communications at once.

The nature of these lasers means that they experience a wavelength drift with a variation in temperature. The consistency of the operation of the laser, therefore, relies on the consistency and effectiveness of a temperature control system or some other system which can counteract the wavelength drift associated with temperature changes.

One particular solution to this problem is a thermo-electric cooling system, which prevents an increasing ambient temperature, or the heat generated by the operation of the laser or adjacent equipment, from affecting the laser's performance. This solution requires the consumption of extra power to provide for the cooling device, and these devices themselves are inefficient.

An alternative method investigated in this report is the continuous re-tuning of the laser by varying its input (drive) current during operation, along with current supplied to supplementary wavelength-selection devices in the case of two-section and Vernier lasers. The amount of current supplied to the laser has a direct affect on its output wavelength, and so this re-tuning can be used to maintain consistent operation without the need for dedicated cooling hardware.

The effect that temperature has on several parameters of the laser devices were initially analysed and compared between their respective approaches to achieving a useful signal for relevant applications.

The series of investigations described in this report found that this method of manual re-tuning could achieve a consistent wavelength within 0.004 nm of a target wavelength with the Vernier laser, the most precise variant tested. Other laser devices showed that a relatively consistent wavelength may be maintained without a compromise on SMSR within a range of 20-60°C.

Acknowledgements

I was helped in the lab with the setting up and calibrating of equipment such as the electronics, microscope and computer by PhD students Caolan Murphy, Robert McKenna and Dovydas Mickus. I want to thank them also for their explanations of the operation of the lasers and the related information I needed to know to properly understand what the experiments were achieving.

I thank Sepideh Tayeb Naimi for providing information that I used for simulating data, and for helping me write the Python code used to generate those simulated results. Michael McDermott also provided information that I needed to complete my simulations.

Professor John Donegan oversaw my project and organised the use of the labs and included me in weekly meetings to review the data I was taking in the lab. I want to thank him for that, and for reviewing several drafts of this report, recommending the changes I needed to make to improve my report.

Contents

1	Introduction	1
2	Background and Theory	2
2.1	Fundamental semiconductor processes	2
2.2	Heterostructures and Laser Fabrication	3
2.3	Rate Equations	4
2.4	The laser cavity	4
2.5	Selection of wavelengths	7
2.5.1	The Vernier Laser	9
2.6	Laser parameters	10
2.7	Athermalisation	12
3	Method	14
3.1	Experimental	14
3.1.1	Constant Temperature Characterisation	14
3.1.2	Varied Temperature Characterisation	15
3.1.3	Athermalisation	15
3.2	Simulation	15
3.2.1	Constant Temperature	15
3.2.2	Varied temperature	16
4	Results and discussion	17
4.1	Constant-temperature Data	17
4.1.1	Fabry-Perot Cavity	17
4.1.2	Single-Mode Laser	19
4.1.3	Vernier Laser	21
4.2	Temperature-dependence of wavelength	22
4.2.1	Fabry-Perot Cavity	22
4.2.2	Single-Mode Laser	22
4.3	Temperature-dependence of parameters	24

4.3.1	Fabry-Perot Cavity	24
4.3.2	Single-Mode Laser	24
4.3.3	Vernier Laser	29
4.4	Athermalisation	30
4.4.1	Fabry-Perot cavity	30
4.4.2	Single-Mode Laser	32
4.4.3	Vernier Laser	33
5	Conclusions	36
A1	Appendix	38

List of Figures

2.1	The three optical processes that may occur within the semiconductor. From left to right: Absorption, spontaneous emission and stimulated emission. The bandgap energy E_g is given by: $E_g = E_c - E_v$	2
2.2	Energy band diagram of the double heterostructure arrangement.	3
2.3	Basic structure of a laser diode. There is 'sandwich' of p-type layers and n-type lasers, and an active region between them. The active region is where recombination takes place, and also acts as the lasing cavity. Electrodes provide current (carrier pump) to the device.	3
2.4	A diagram of a Fabry-Perot laser cavity.	5
2.5	An example of a gain curve generated by a lasing Fabry-Perot cavity. This spectrum was generated by a 700 micron device. The laser has no devices to filter wavelengths, and all modes are visible in the spectrum, within the gain envelope of the laser.	6
2.6	Left: The possible resonating modes within a laser cavity and Right: The gain curve which determines which modes are actually expressed in the spectrum of light generated by the device.	6
2.7	8
2.8	Diagram of a Vernier laser.	9
2.9	The first row of plots include the separate grating modes, while the second row shows the resulting spectrum of the Vernier laser. These plots were not taken from data for this report.	10
2.10	A set of LI curves corresponding to different laser devices.	11
2.11	SMSR indicated on a spectrum from a single-mode laser.	12
2.12	13
4.1	The peaks of spectra taken from the FP vs. the current input into the device.	17
4.2	The LI curve generated by the 1.5 micron Fabry-Perot laser.	18
4.3	The LI simulated by the Python script.	18
4.4	A spectrum taken from the single-mode device.	19
4.5	Plots of peak wavelength vs drive current for the single-mode laser.	20

4.6	LI curves generated by the 700 micron laser, corresponding to several currents applied to the SOA section.	21
4.7	LI curve of the Vernier laser at 20°C.	21
4.8	22
4.9	22
4.10	Peak wavelength vs. Temperature of the single-mode laser for 4 SOA currents at drive currents of 50mA and 80mA.	23
4.11	LI curves of a Fabry-Perot cavity operating at 1.5 microns, categorised by temperature.	24
4.12	LI curves corresponding to different temperatures, generated by the 700 micron single-mode laser.	25
4.13	Threshold current vs. Temperature for the 700 micron single-mode laser. . .	25
4.14	Simulated threshold current vs. temperature. A shallower, but similarly shaped curve was generated for the relationship.	26
4.15	Another simulation, run with different parameters and constants, demonstrates the curve more distinctly.	26
4.16	Slope efficiency vs. Temperature for the 700 micron single-mode laser. . .	27
4.17	28
4.18	Combined LI curves taken from the 700 micron single-mode laser array, categorised by temperature.	28
4.19	Slope efficiency of the Vernier device vs. temperature.	29
4.20	Data relating to the athermalisation of the 700 micron Fabry-Perot cavity. .	30
4.21	Data relating to the athermalisation of the 700 micron single-mode laser. .	32
4.22	Data from first quasi-continuous tuning of the Vernier laser, at 1546.888 nm initial wavelength - temperature, in Celsius, along x-axis.	33
4.23	Data from second quasi-continuous tuning of the Vernier laser, at 1575.364 nm initial wavelength.	34
4.24	Data from third quasi-continuous tuning of the Vernier laser, at 1569.596 nm initial wavelength.	35
A1.1	Python code used to generate the simulated non-temperature-dependent LI curves.	38
A1.2	Python code used to generate the simulated non-temperature-dependent LI curves.	39
A1.3	Python code used to generate temperature-dependent laser parameters. . .	39

1 Introduction

There are various designs of semiconductor lasers that are used in modern communications systems. The basic form of the semiconductor laser is the Fabry-Perot setup, where two mirrors flank the semiconductor active region. The other designs are additions to this setup with added devices for both the selection of wavelengths from a range generated by a Fabry-Perot device and the amplification of those signals. Characterisation of laser diodes operating under different conditions and with different configurations can highlight certain trends; the thresholds that must be reached in terms of carriers supplied to the semiconductor materials, the efficiency of the operation of the laser and, most important for the consistent operation under temperature changes, the nature of the variation of certain consequential parameters with temperature.

One application of single-mode laser diodes in optical communications is part of wavelength division multiplexing systems (WDM). A WDM system requires discrete wavelength channels in series within a fibre, and it is necessary that these channels do not shift into each-other's wavelength range. Wavelength drift with temperature change is a technical challenge with such systems, with even small variations in temperature leading to functional issues - wavelength drift occurs at a rate of $0.1 \text{ nm } ^\circ\text{C}^{-1}$. In order to keep a signal coherent within each channel, this variation must be prevented.

2 Background and Theory

2.1 Fundamental semiconductor processes

The properties of semiconductor materials are what allow for the operation of diode lasers. In all semiconductors, a bandgap energy exists between a conduction band and valence band, which correspond to bands of possible electron energy states within the material. The transition of electrons from the valence band to the conduction band requires at least the energy E_g to be gained by the electron. There are three optical processes that may occur due to this bandgap; two of which result in the emission of a photon [1]. Figure 2.1 contains an illustration of each optical process and the energy levels involved.

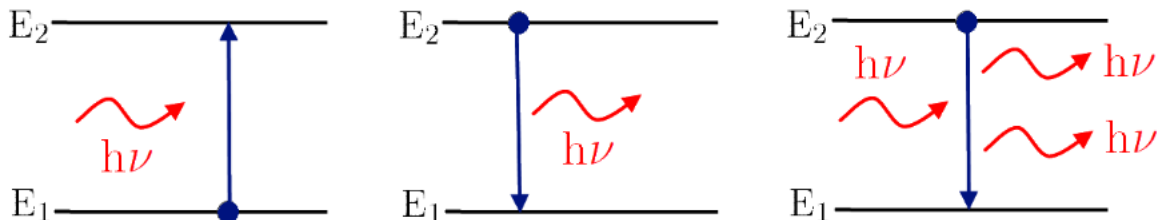


Figure 2.1: The three optical processes that may occur within the semiconductor. From left to right: Absorption, spontaneous emission and stimulated emission. The bandgap energy E_g is given by: $E_g = E_c - E_v$.

A photon may be absorbed by the material, where the photon energy equals that of the bandgap energy E_g , and the energy is used to promote an electron to the conduction band, generating a hole in the valence band. Spontaneous emission occurs when an electron in an excited state releases energy and moves into the valence band of the semiconductor. Energy

corresponding to E_g is released in the form of a photon. There is a recombination of the electron and the hole in the valence band - the hole is no longer present.

Stimulated emission is the recombination of the electron-hole pair that is prompted by the incidence of a photon. In such a process, one photon is incident, the electron is stimulated to recombine with the hole in the valence band, and two photons are subsequently emitted. This optical process is what allows optical gain to occur within semiconductor materials - the fundamental operating principle of the laser.

2.2 Heterostructures and Laser Fabrication

In order to control the location of recombination to, in turn, control where photons are emitted, modern devices utilise a double heterostructure scheme.

The double heterostructure includes an active region of lower bandgap energy positioned between two regions of relatively higher bandgap energy. There exists high bandgap confinement layers either side of this active region - electrons and holes are forced to recombine in the active region.

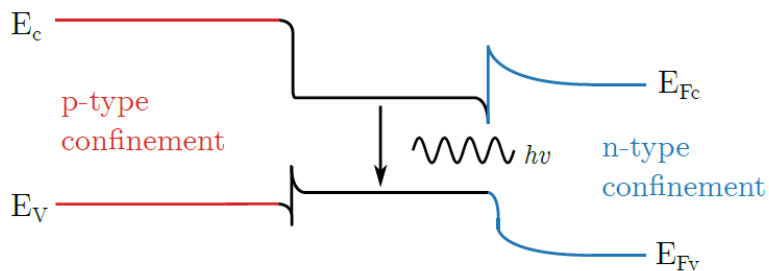


Figure 2.2: Energy band diagram of the double heterostructure arrangement.

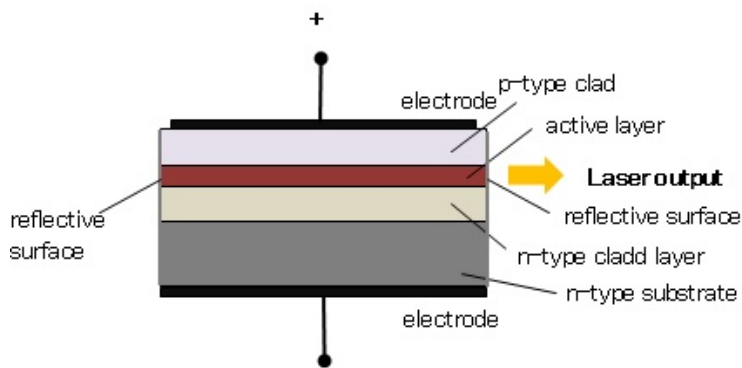


Figure 2.3: Basic structure of a laser diode. There is 'sandwich' of p-type layers and n-type lasers, and an active region between them. The active region is where recombination takes place, and also acts as the lasing cavity. Electrodes provide current (carrier pump) to the device.

2.3 Rate Equations

To achieve consistent production of photons with significant output of energy (lasing) from a diode, the number of electrons in the conduction band of the material needs to be higher than the number in the valence band. This is referred to as 'population inversion' and can only be caused by the introduction of energy to the system from an external source.

In laser diodes, electrons are pumped from the valence band into the conduction band, to generate the spontaneous emission, as these carriers recombine in the valence band, to cause the stimulated emission necessary for the device to achieve lasing.

The overall rate at which photons are generated by these optical processes combined is given by:

$$\frac{dN}{dt} = \frac{I\eta_i}{Vq} - (AN + BN^2 + CN^3 + R_{stim}) \quad (1)$$

where: I is the injection current, q is the magnitude of the charge of the electron, V is the volume of the laser's active region and η_i is the injection efficiency of carriers [1].

A , B and C are coefficients that correspond to the non-radiative recombination processes that take place in the material.

2.4 The laser cavity

The laser cavity functions in a laser diode in the same way it functions in other conventional laser devices. The cavity is used to allow the generated light to re-enter the material, the gain medium to trigger further stimulated emission of photons by the reflection of the light off of mirrors on opposite sides of the resonating chamber. This creates significant population inversion of the charge carriers and a subsequent strong gain in the material - the use of the cavity also generates distinct resonating modes within it, with an associated gain curve containing individual standing wave modes. This simplest form of laser cavity is called a Fabry-Perot cavity. Mirror reflectivity may be varied to alter the output of the laser.

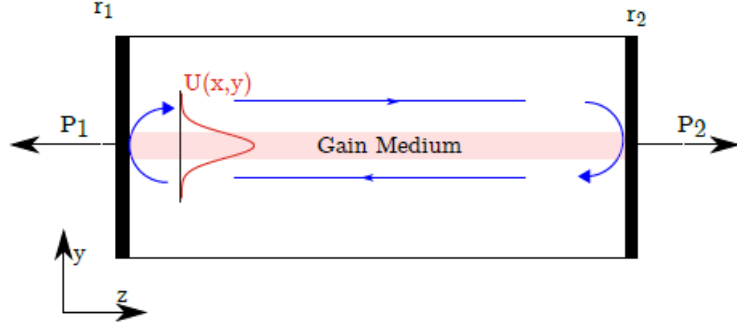


Figure 2.4: A diagram of a Fabry-Perot laser cavity.

In order for the material to produce a significant output of light consistently, the optical gain needs to exceed the losses at either end (mirrors) of the resonating chamber - the round-trip gain condition[1].

β is the propagation constant, which is used to characterise the behaviour of the light inside the cavity (Equation 1).

$$\beta = \kappa_0 n'_{\text{eff}} + j \frac{g_{\text{net}}}{2} \quad (2)$$

$$g_{\text{net}} = g\Gamma - \alpha; \quad (3)$$

$$\kappa_0 = \frac{2\pi}{\lambda} \quad (4)$$

where Γ is the confinement factor, g_{net} is the net modal gain, α is the waveguide loss and κ is the free space propagation constant.

Round trip gain condition:

$$r_1 r_2 e^{-2iL\beta} = 1 \quad (5)$$

The Fabry-Perot cavity generates an emission spectrum in a relatively wide profile of individual thin peaks which correspond to the cavity's longitudinal resonant modes.

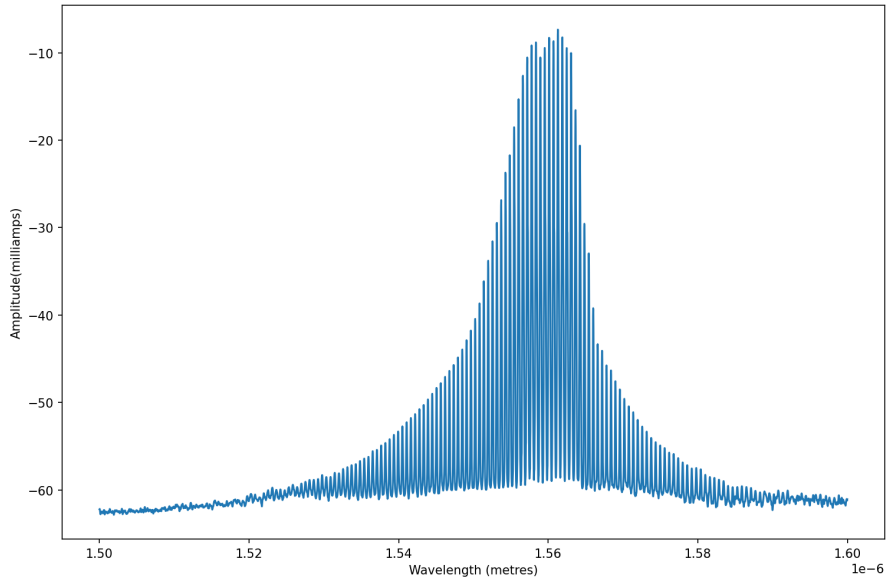


Figure 2.5: An example of a gain curve generated by a lasing Fabry-Perot cavity. This spectrum was generated by a 700 micron device. The laser has no devices to filter wavelengths, and all modes are visible in the spectrum, within the gain envelope of the laser.

The multitude of peaks within the spectrum are clearly visible, and the existence of these significant peaks makes the use of unaltered Fabry-Perot lasers insufficient for optical communications applications, which require finer tuning and the exclusion of wide portions of the gain spectrum.

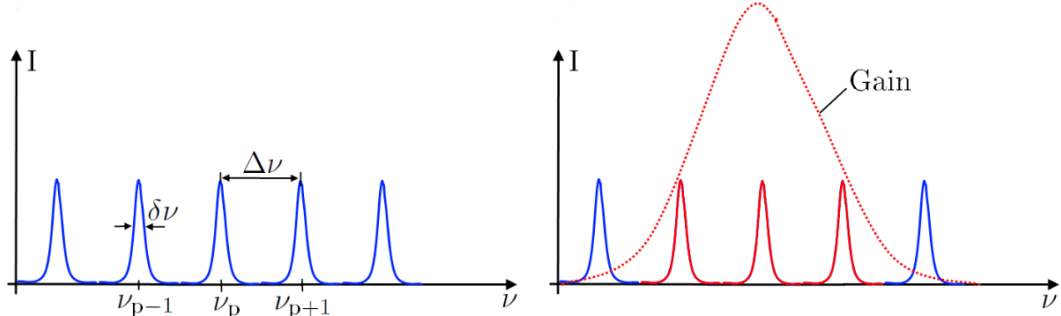


Figure 2.6: Left: The possible resonating modes within a laser cavity and Right: The gain curve which determines which modes are actually expressed in the spectrum of light generated by the device.

The separation of resonating modes in the cavity, $\Delta\nu$, is given by:

$$\Delta\nu = \frac{c}{2nL} \quad (6)$$

Where n is the refractive index of the active region, L is the length of the cavity, and c is the speed of light.

2.5 Selection of wavelengths

Wavelength selection with a Fabry-Perot laser is a simple process by which the input current is changed, thus affecting the refractive index, and the wavelength produced by the laser. Equation 7 relates the refractive index change with the injection of carriers into the material (Free Carrier Plasma effect) [2].

$$\Delta n' = -\frac{e^2 \lambda^2}{8\pi^2 c^2 n \epsilon_0} \left(\frac{1}{m_e + \frac{1}{m_h}} N \right) \quad (7)$$

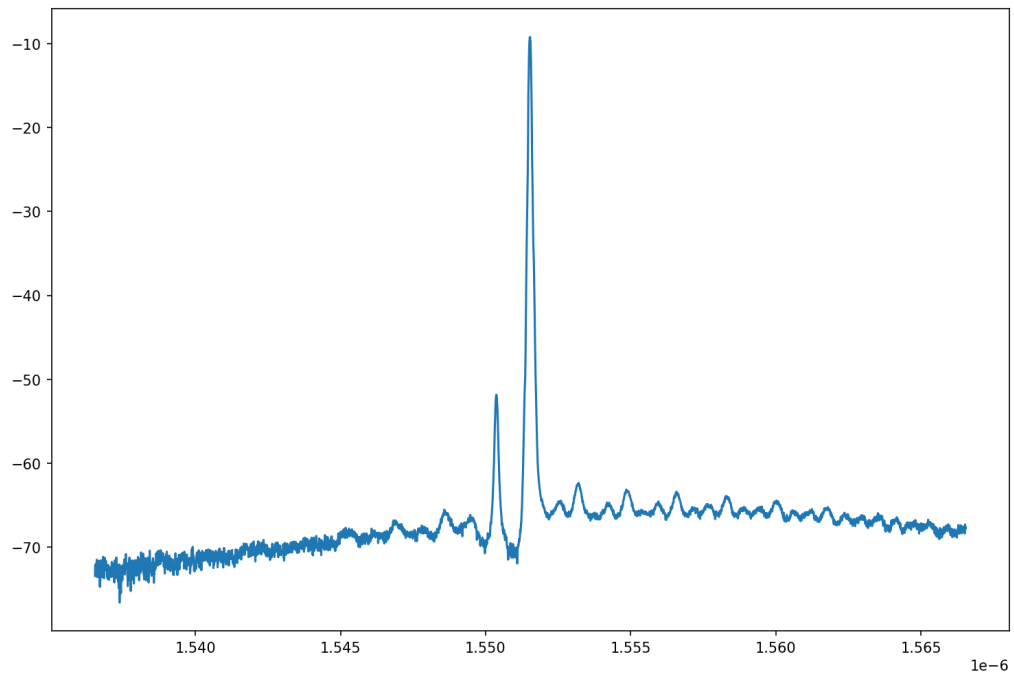
In equation 7, N is the carrier density, m_e is the effective mass of the electron, m_h is the effective mass of the hole, e is the charge of an electron, c is the speed of light, and ϵ is the permittivity of free space.

Greater N decreases the refractive index, causing a linear blue-shift in wavelength in the cavity with increased current.

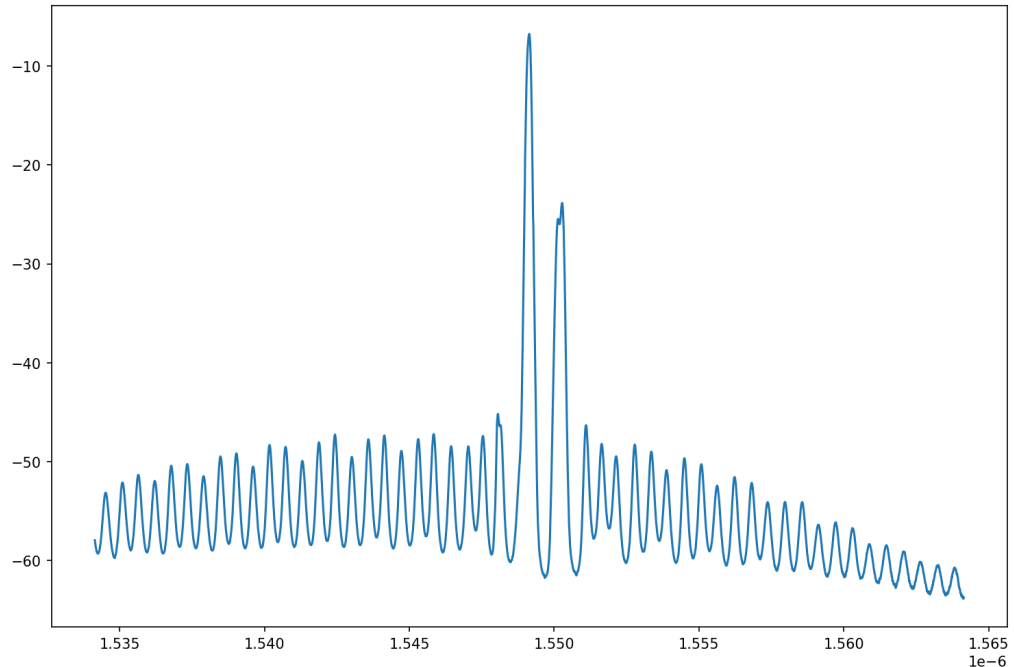
Changes in temperature also affect the spectrum output by a Fabry-Perot laser - the refractive index increases with temperature, as phonon-electron interactions will cause a decreased bandgap energy. This process causes a red-shift in the wavelengths present in the cavity[3].

To confine the laser to a strict single-mode operation, a common method is the use of a Distributed Bragg Reflector (DBR). This is a length of grating with a set period between slots. The DBR functions to select a specific wavelength out of those resonant frequencies constitute the gain curve. The wavelength to be selected is one so that the reflections of that wavelength within the Bragg grating will interfere constructively (reflecting back into the resonating cavity) while others in the gain envelope ideally interfere destructively and do not re-enter the cavity to further resonate or add to lasing. In practice, some wavelength peaks near to the selected wavelength will usually experience low enough losses to achieve threshold (gain condition) within the cavity.

The spectrum of a laser with a DBR section demonstrates a sharp peak at a particular wavelength within the gain curve, and very little to none other noticeable features.



(a) A typical spectrum from a single-mode laser. This spectrum was recorded from a single-mode device operating at a wavelength of approximately 1.5 microns.



(b) A single-mode laser spectrum recorded as the laser is beginning to lase in an adjacent mode; two significant peaks are visible. The grating of the device and the device itself can be supplied with greater current to 'mode hop' to the next possible lasing mode.

Figure 2.7: .

2.5.1 The Vernier Laser

Vernier lasers utilise a combination of the effects of two grating sections to achieve a wider range of tuning than a 2-section single-mode laser. The Fabry-Perot resonance cavity is located between the two sections, generating a gain curve. These grating sections have differing periods, and they will 'select' a set of wavelengths or peaks - as with a basic single-mode laser - from this curve - these peaks will interfere constructively if they coincide with each-other. The spectrum still remains within the gain curve of the cavity itself.

The modes available to the Vernier device may be characterised by their mode spacing. The quasi-continuous range of the Vernier laser, or the 'super FSR' is given by:

$$\Delta\lambda_s = \frac{\Delta\lambda_f\Delta\lambda_b + 1}{\Delta\lambda_b - \Delta\lambda_f} \quad (8)$$

where Δ_f and Δ_b are the FSR values (the mode separation) for the front and back grating sections, respectively [4].

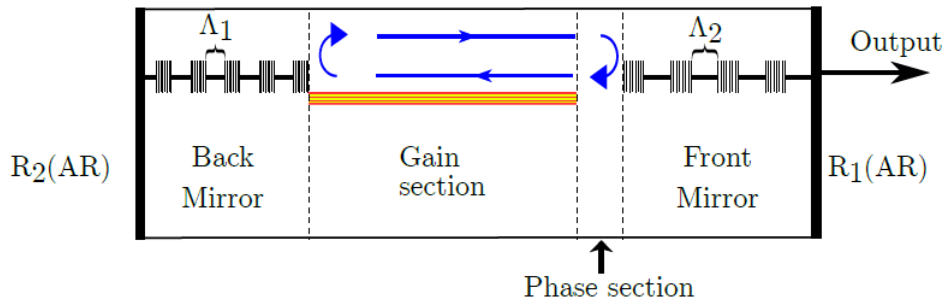


Figure 2.8: Diagram of a Vernier laser.

Figure 2.9 shows the spectrum of available modes corresponding to the two grating sections of the Vernier laser on the same plot, and the resulting spectrum when these gratings spectra are combined; the result of constructive interference where peaks coincide and destructive interference where they do not.

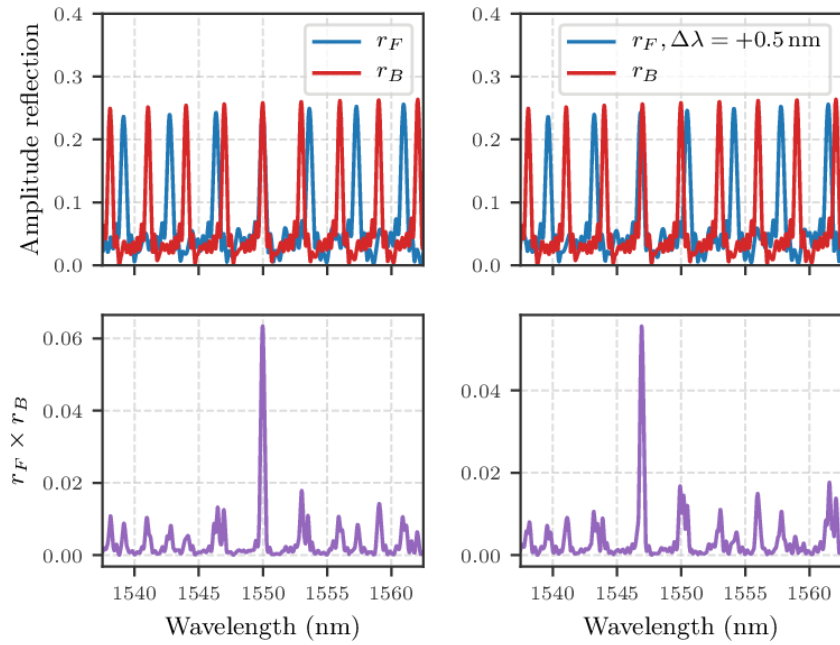


Figure 2.9: The first row of plots include the separate grating modes, while the second row shows the resulting spectrum of the Vernier laser. These plots were not taken from data for this report.

2.6 Laser parameters

A laser can be characterised by the examining of a few key parameters and behaviours relating primarily to its output intensity at a range of input currents. The threshold current is the input current that is required to allow lasing to occur, and the ratio of output intensity versus the input (drive) current's power is referred to as the slope efficiency of the laser.

$$\eta_{sl} = \frac{I_{Input}}{I_{Photons}} \quad (9)$$

I_{Input} is the input current's power and $I_{Photons}$ is the light intensity generated.

$$I_{th} = \frac{qN_{th}}{\tau_c} \quad (10)$$

Where: N_{th} is the carrier threshold for lasing, q is the magnitude of charge of the electron, and τ_c is the carrier lifetime.

An LI curve may be generated from a set of input currents and the measured outputs of a device which can directly illustrate these particular characteristics of the laser. It plots the light intensity generated by the laser vs. the current supplied to it. The LI plot can clearly graphically demonstrate the sudden increase in output power after some current threshold

for that device.

Shown in figure 2.10 are three LI curves that were generated, respectively, by a Fabry-Perot (single-section) laser cavity, a single-mode laser, and a Vernier laser.

A line graph titled "Fabry-Perot LI curve". The y-axis is labeled "Output Current (mA)" and ranges from 0.0000 to 0.0040. The x-axis is labeled "Drive Current (mA)" and ranges from 0 to 35. The curve shows a sharp increase in output current starting around 14 mA, reaching approximately 0.0040 mA at 33 mA.

(a) LI curve for a 700 micron Fabry-Perot laser.

A line graph titled "LI plots for 700 micron, triple-period slotted laser array [Device 4211_3]". The y-axis is labeled "Output current (A)" and ranges from 0.000 to 0.008. The x-axis is labeled "Input Current (mA)" and ranges from 20 to 100. Six curves are shown for different temperatures: 20°C (blue), 30°C (orange), 40°C (green), 50°C (red), 60°C (purple), and 80°C (pink). All curves show a sharp increase in output current starting at different input currents (around 25-30 mA for 20°C and 40°C, around 40 mA for 30°C, around 55 mA for 50°C, around 70 mA for 60°C, and around 90 mA for 80°C).

(b) LI curves for a single-mode laser operating at different temperatures.

A line graph titled "Vernier Laser LI curve, 50°C". The y-axis is labeled "Photocurrent (A)" and ranges from 0.0000 to 0.0010. The x-axis is labeled "Drive Current (mA)" and ranges from 125 to 325. A single blue curve shows a sharp increase in photocurrent starting around 200 mA, reaching approximately 0.0010 A at 325 mA.

(c) LI curve of a Vernier laser at 50°C.

Figure 2.10: A set of LI curves corresponding to different laser devices.

11

The overall effectiveness of the laser in terms of its ability to select a single wavelength in exclusion of others is characterised by the SMSR (Single Mode Suppression Ratio) which is the measurement of the intensity of the largest and second-largest peaks in the laser spectrum. This parameter is not of significant concern in determining the temperature-dependence of other important features, but a laser used for communications is required to have very little noise. The SMSR is therefore an important aspect to monitor when carrying out athermalisation of the laser across a range of temperatures for any communications application.

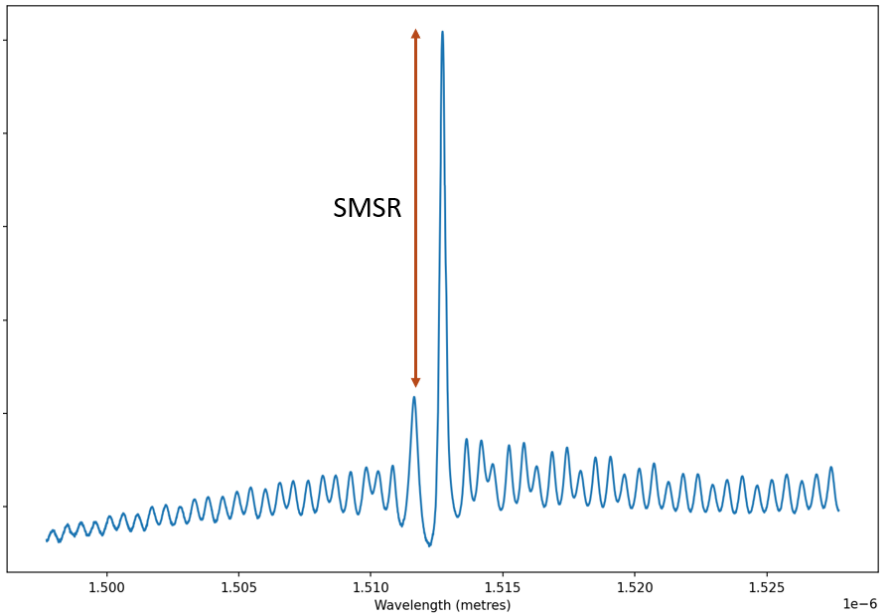


Figure 2.11: SMSR indicated on a spectrum from a single-mode laser.

2.7 Athermalisation

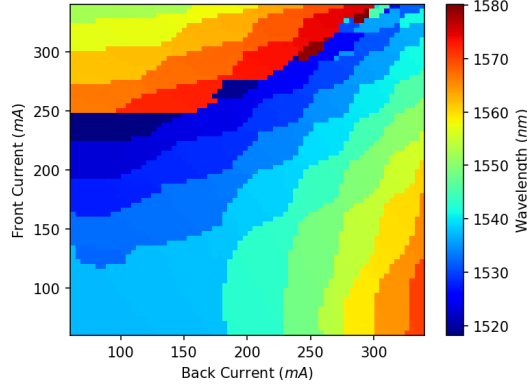
The parameters of a laser, and therefore the frequency of its output, will vary as the laser is heated or cooled, and the laser itself generates heat by its own operation. To operate effectively and consistently, the laser must therefore be tuned in some way to keep these parameters as constant as possible across a range of temperatures.

Athermalisation of a laser; the maintaining of the laser within a certain operational constriction while experiencing a variation in temperature, involves the quasi-continuous re-tuning of the device as the temperature change is occurring.

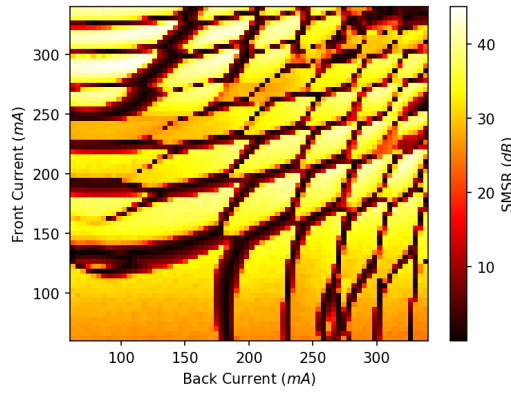
Modes accessible to the laser are inherently discrete, and so a continuous re-tuning of the device to achieve a continuous wavelength range is only possible with a small range of wavelengths.

For the Vernier laser, a tuning map can demonstrate the modes that are accessible to the

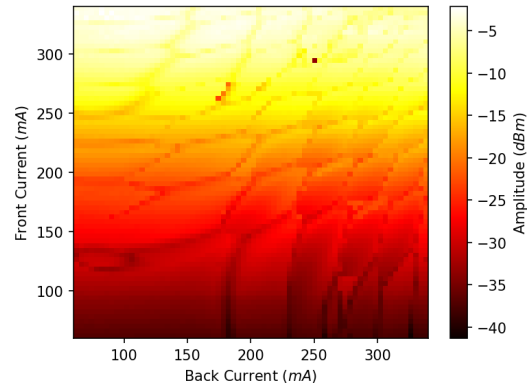
device. The modes visible as 'supermodes'; positions where the allowed modes of the gratings overlap. The tuning map for the Vernier laser used in the athermalisation experiments is shown in figure 2.12.



(a) Tuning map of vernier laser, wavelength heat-map with grating currents indicated on the axes, at constant temperature.



(b) SCSR of all spectra in the tuning map.



(c) Peak amplitude of all spectra in the tuning map.

Figure 2.12: .

Altering the current of both gratings of the device allows maintaining the laser within a particular mode. As the laser is heated, the positions of these modes on the tuning map will shift, and the current must be varied to compensate for this.

3 Method

3.1 Experimental

3.1.1 Constant Temperature Characterisation

Firstly, the spectra of a simple Fabry-Perot device of the same length as the FP section used in successive investigations were taken as the input current was increased in increments of 10mA.

For the characterisation of the lasers, initially without a varying operating temperature, the laser diodes were mounted on a viewing platform where a camera and monitor were used to position a photodetector device on front of whichever laser was to be tested. Laser diodes were provided with a current by the use of manually-positioned pins contacting a set of bare metal electrodes on the laser platform. The photodetector was connected to a oscilloscope and, in turn, a computer.

For the recording of spectra of the devices, a Python script was run which collected the spectral data from the oscilloscope, and saved the data with a manually-input corresponding input current value. For each individual instance where a spectrum was taken, this procedure was followed. Relevant peaks were selected from these spectra using a separate Python script outside of the lab.

In the collection of the LI curves of the single-section and two-section lasers, another purpose-built Python script was used to control the power supply output and generate an LI curve across a range of input currents. Several LI curves were generated using the single-mode lasers which corresponded to different SOA currents - which were manually input into the saved data file from the Python script. LI curves for the Fabry-Perot device were generated using input current increments of 2 mA.

The threshold current and slope efficiency corresponding to the LI curves was extracted from the data using a separate Python script outside of the lab.

3.1.2 Varied Temperature Characterisation

A copper block and Peltier device were placed in contact with the underside of the laser diode array. The Peltier device was controlled by a power supply and was used to vary the temperature for relevant data collection.

The collection of spectra and peak data was done in a similar manner to the constant-data investigations, where the spectral data was collected from the oscilloscope by the computer and recorded. The LI curves were generated similarly, with several being taken for increasing temperatures. Threshold current and slope efficiency values were extracted from this data and plotted collectively against temperature to determine their relationship.

3.1.3 Athermalisation

Data for the athermalisation attempts was collected using a Python script that read peak data from an oscilloscope which measured the device output spectrum. There was, at each point where the temperature was changed, a manual re-tuning of the device by altering the current supplied to it, and the data was then recorded using the Python script.

With the two-section (single-mode) laser, there were two sections to which there was current being supplied. With the Vernier device, the Fabry-Perot resonator section was supplied a current, and the two gratings current supplies were varied independently to achieve the desired peak location on the spectrum. The recording of athermalisation data for all devices followed a procedure of temperature change, manual tuning, and then the use of the Python script to extract the position of the spectral peak.

3.2 Simulation

3.2.1 Constant Temperature

Simulations of these parameters were generated using a Python script for comparison with experimental data and the extracted parameters.

The script used to generate the LI curves for the laser diode used in the experiments was written in Python. The following are the formulae which were used in writing that script:

Effective mirror loss:

$$\tilde{\alpha}_m = \frac{1}{L} \log\left(\frac{1}{\sqrt{R_1 R_2}}\right) \quad (1)$$

Output coupling efficiency:

$$\eta_o = \frac{\tilde{a}_m}{\tilde{a}_m + \tilde{a}} \quad (2)$$

The photon lifetime in cavity:

$$\frac{1}{\tau_p} = v_g [\tilde{a}_m + \tilde{a}] = \frac{v_g}{L} \log\left(\frac{1}{\sqrt{R_1 R_2}}\right) + v_g \tilde{\alpha} \quad (3)$$

Threshold gain:

$$\Gamma_a v_g \tilde{g}_{th} = \frac{1}{\tau_p} \quad (4)$$

Threshold carrier density:

$$n_{th} = n_{tr} e^{\frac{\tilde{g}_{th}}{\tilde{g}_0}} \quad (5)$$

Threshold current:

$$\frac{\eta_i I_{th}}{q V_a} \approx A n_{th} + B n_{th}^2 + C n_{th}^3 \quad (6)$$

Laser power:

$$P = \eta_o \eta_i \frac{\hbar \omega}{q} \quad (7)$$

3.2.2 Varied temperature

In the same manner as the simulation for the parameters of the laser without temperature variation, the variation of these parameters was simulated using a Python script. These simulations for both scenarios were run for the purpose of demonstrating an overall trend to be expected rather than actual numerical results, as the inclusion of gratings in the lasers used in the experiments, among other factors, meant that these simulations were inaccurate, in detail.

4 Results and discussion

4.1 Constant-temperature Data

4.1.1 Fabry-Perot Cavity

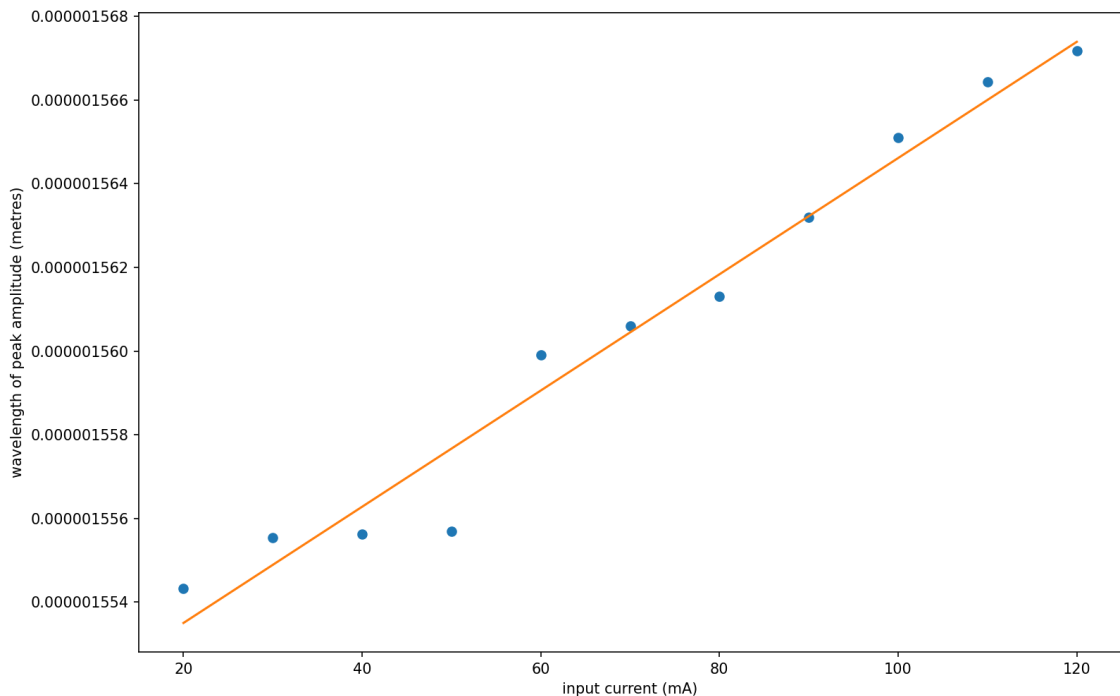


Figure 4.1: The peaks of spectra taken from the FP vs. the current input into the device.

The spectra taken from the Fabry-Perot cavity of length 700 microns featured the relatively wide spectrum of significant peaks that was expected. An example of this form of spectrum is shown in figure 2.5. There was a clear linear increase in the wavelength corresponding to the peak in the spectra as the current was raised (see: figure 4.1).

There is only one corresponding LI curve which can be generated from a Fabry-Perot cavity; the curve for the device used in the lab is shown in figure 4.2.

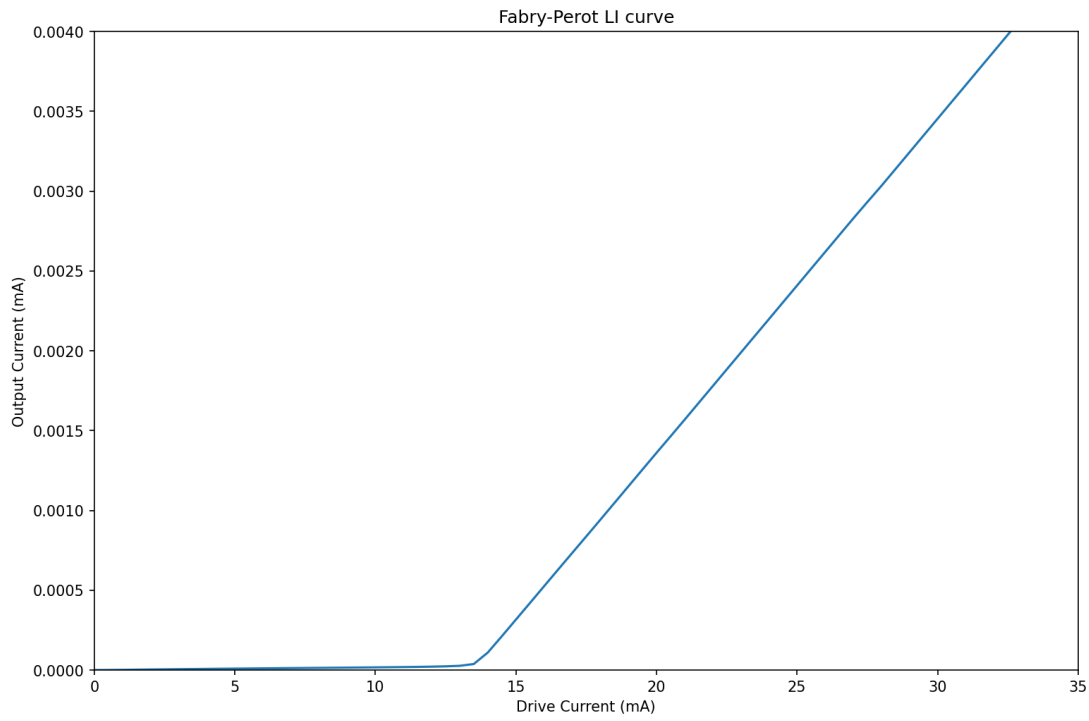


Figure 4.2: The LI curve generated by the 1.5 micron Fabry-Perot laser.

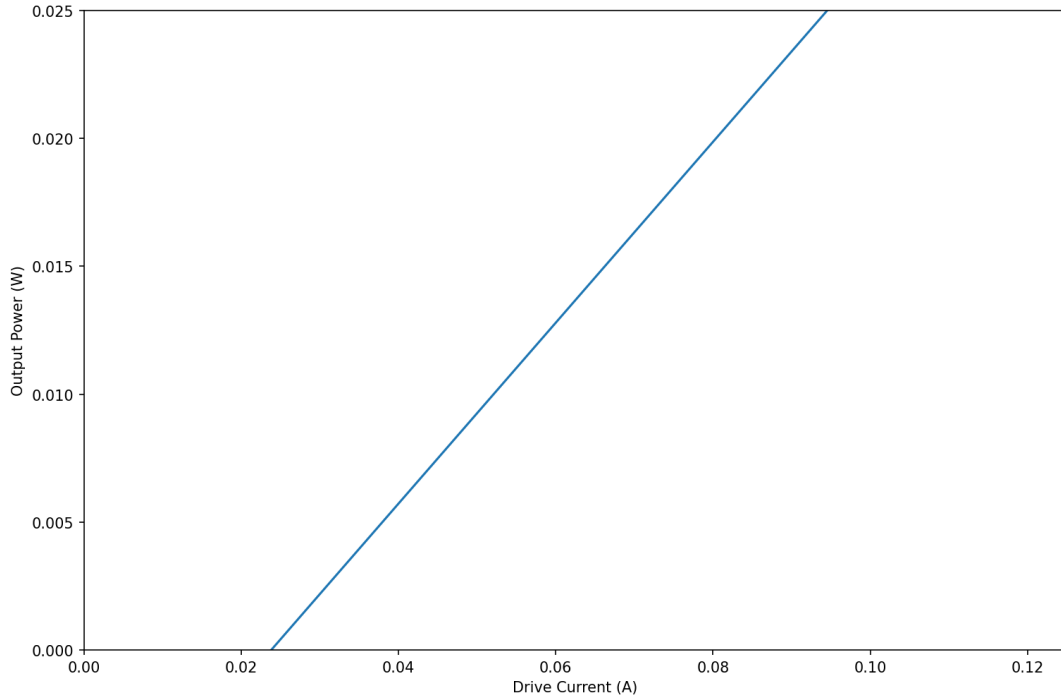


Figure 4.3: The LI simulated by the Python script.

The observed and simulated LI curves for the Fabry-Perot cavity itself agree to a reasonable extent. The threshold current simulated was 23 mA, and the slope efficiency 0.35. The recorded values were 13.5 mA and 0.274.

4.1.2 Single-Mode Laser

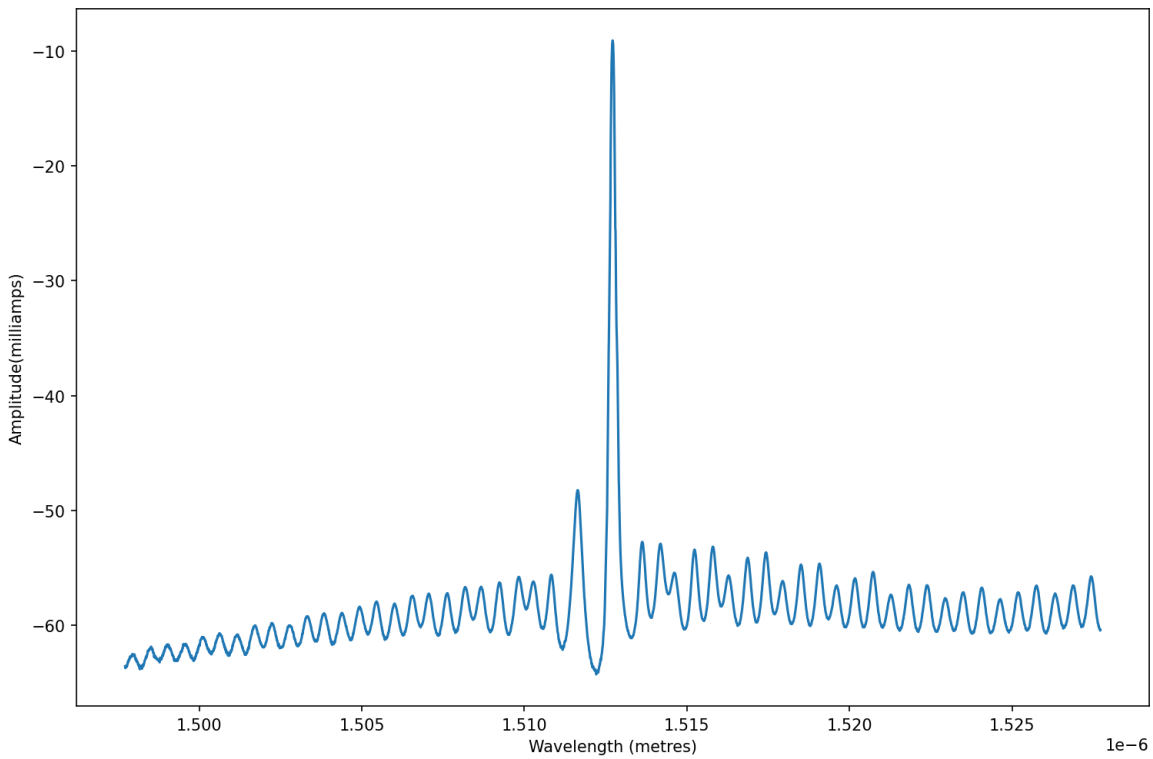
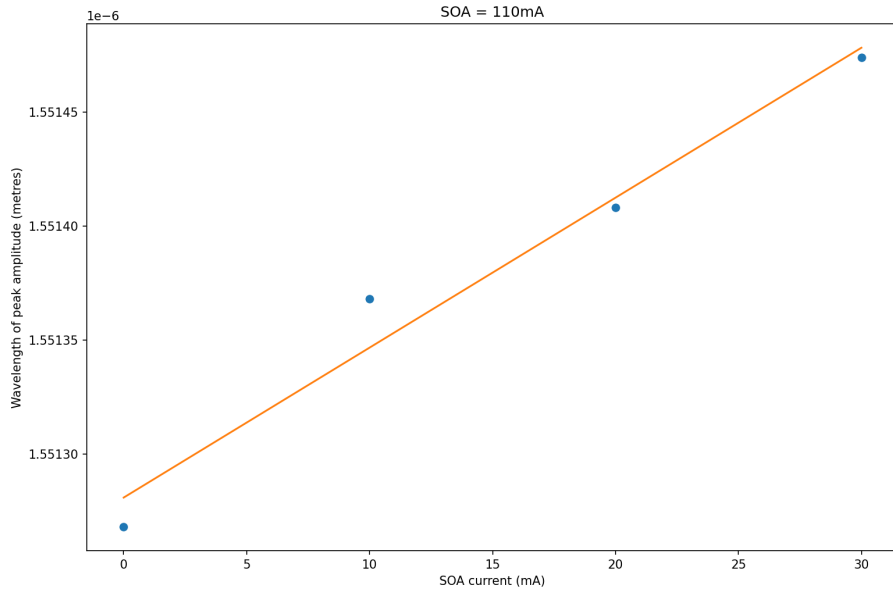
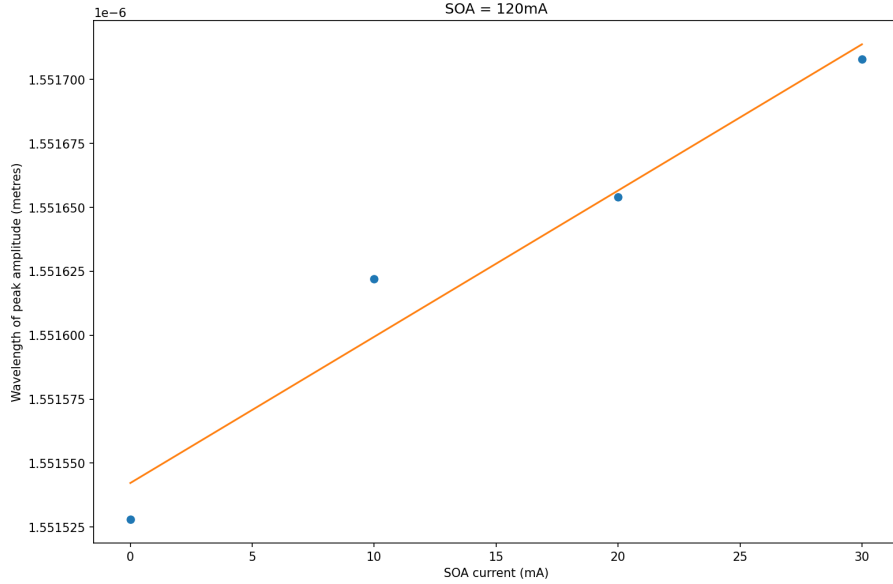


Figure 4.4: A spectrum taken from the single-mode device.

Sharper peaks were generated by the two-section laser, as expected. Peaks followed the same trend as in the case Fabry-Perot cavity - wavelength of peaks increased with an increase in supplied current (see: figure 4.5).



(a) Peak wavelength vs. drive current at SOA current of 110mA.



(b) Peak wavelength vs. drive current at SOA current of 120mA.

Figure 4.5: Plots of peak wavelength vs drive current for the single-mode laser.

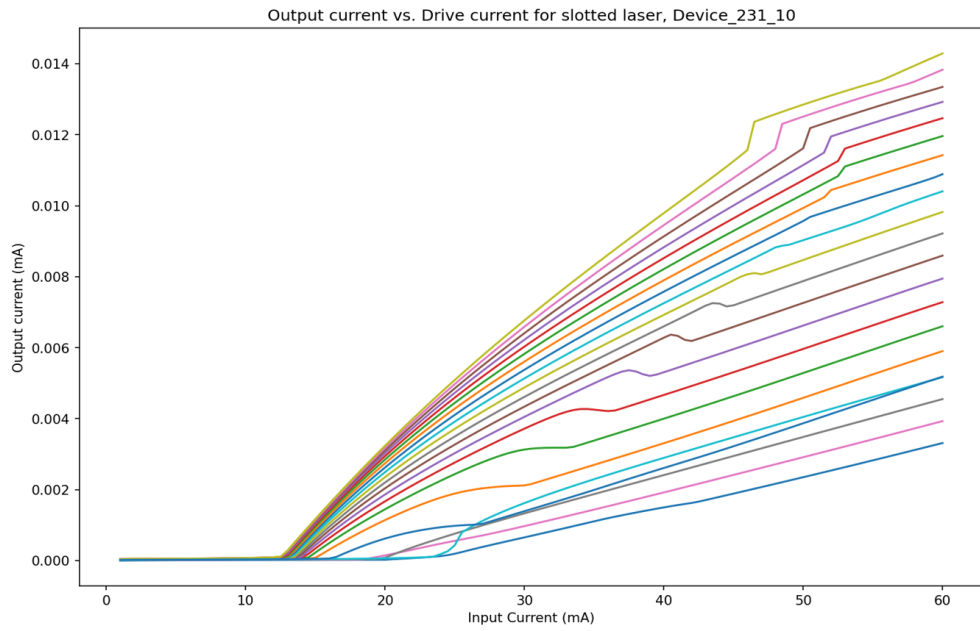


Figure 4.6: LI curves generated by the 700 micron laser, corresponding to several currents applied to the SOA section.

4.1.3 Vernier Laser

The room-temperature LI curve of the vernier device used in the athermalisation experiments is shown in figure. The shape of the LI curve maintains the form and all key features of the LI curves of the other devices.

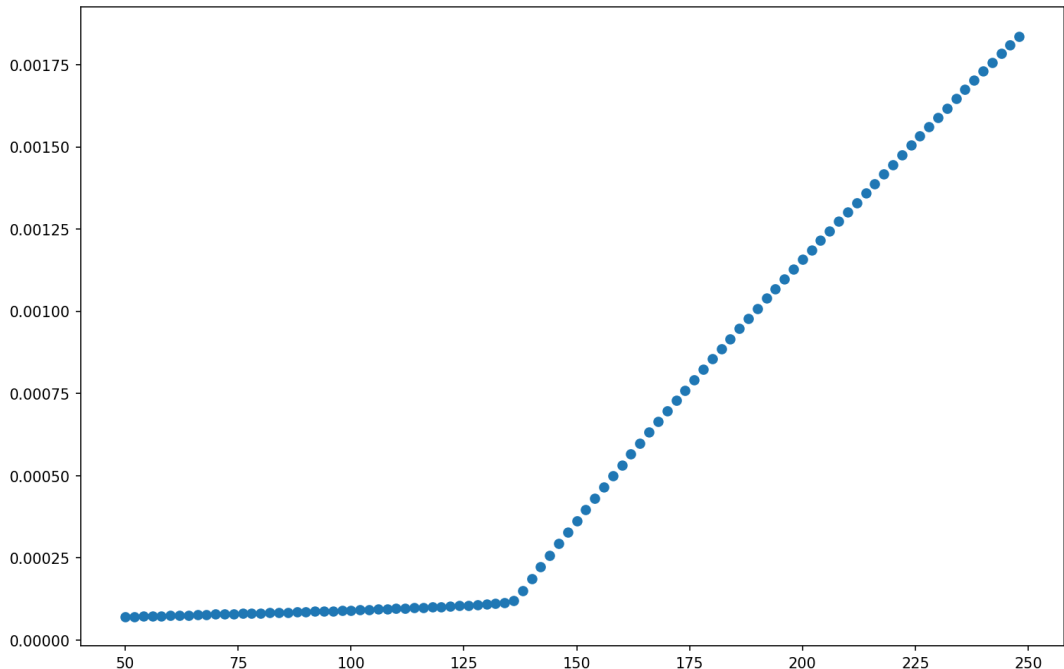
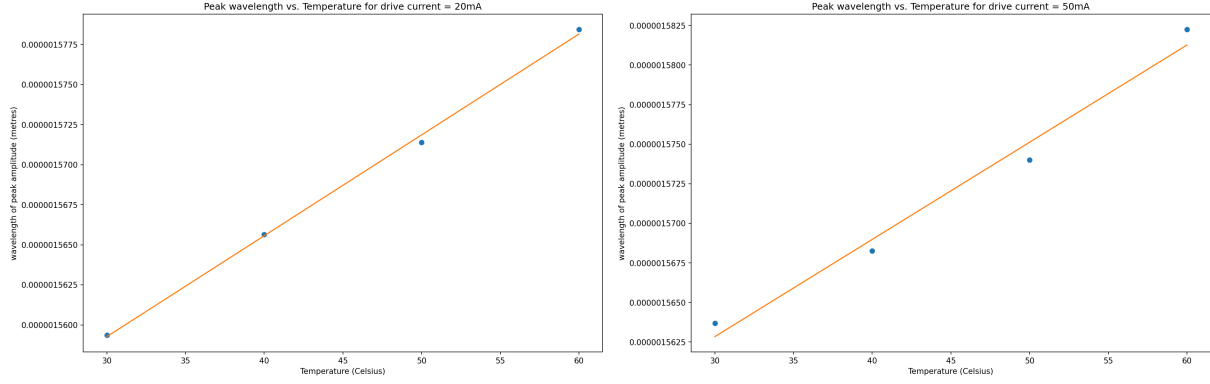


Figure 4.7: LI curve of the Vernier laser at $20^\circ C$.

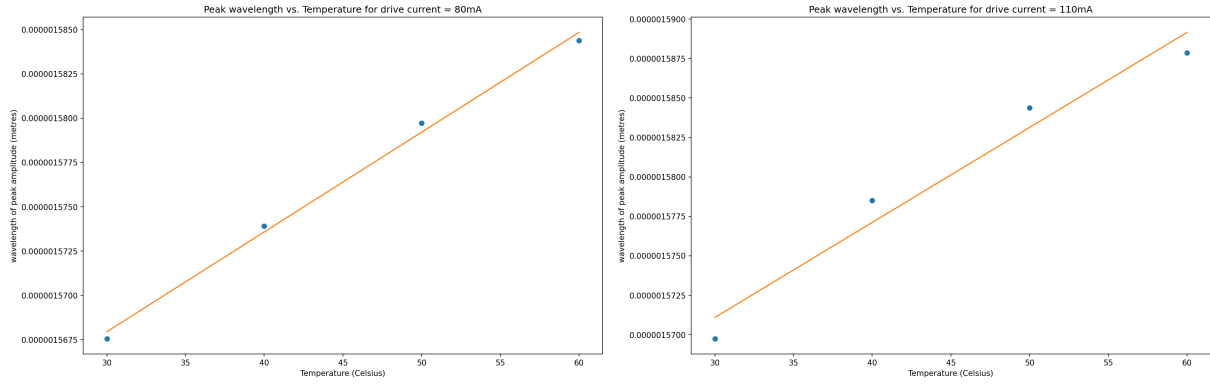
4.2 Temperature-dependence of wavelength

4.2.1 Fabry-Perot Cavity



(a) Peak wavelength vs. temperature at 20mA. (b) Peak wavelength vs. temperature at 50mA.

Figure 4.8: .



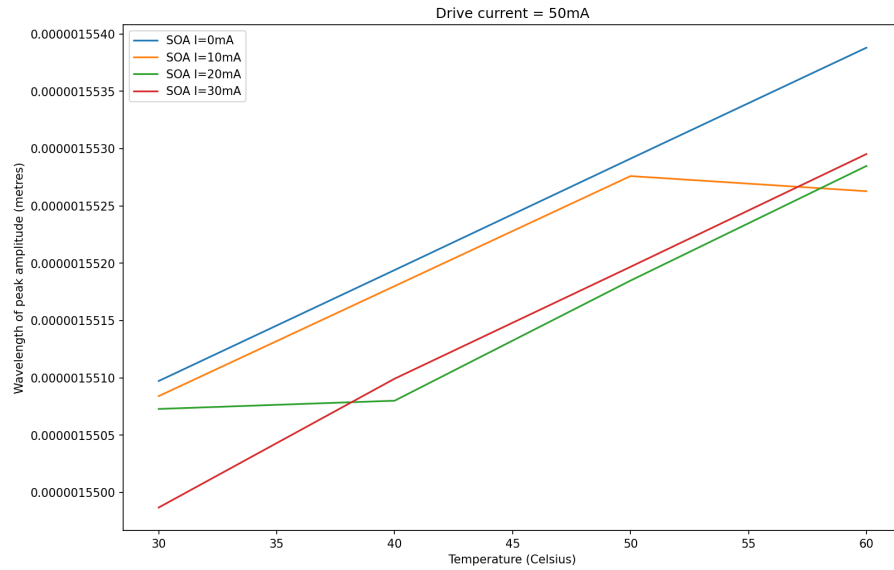
(a) Peak wavelength vs. temperature at 80mA. (b) Peak wavelength vs. temperature at 110mA.

Figure 4.9: .

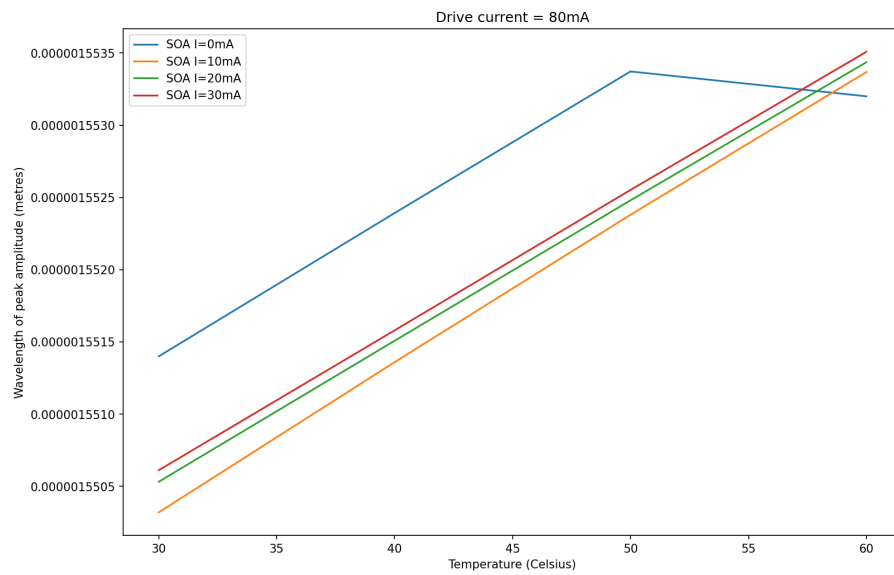
The relationship between wavelength and temperature for the Fabry-Perot was a clear, negative linear relationship. This property was recorded for several currents supplied to the laser and was consistent.

4.2.2 Single-Mode Laser

Figure 4.10 contains the peak wavelengths recorded from the single-mode laser vs temperature, for a small range of SOA currents.



(a) Drive current of 50mA.



(b) Drive current of 80mA.

Figure 4.10: Peak wavelength vs. Temperature of the single-mode laser for 4 SOA currents at drive currents of 50mA and 80mA.

The single mode laser, as with the Fabry-Perot cavity alone, experiences an increase in the frequency of its output with an increase in temperature.

4.3 Temperature-dependence of parameters

4.3.1 Fabry-Perot Cavity

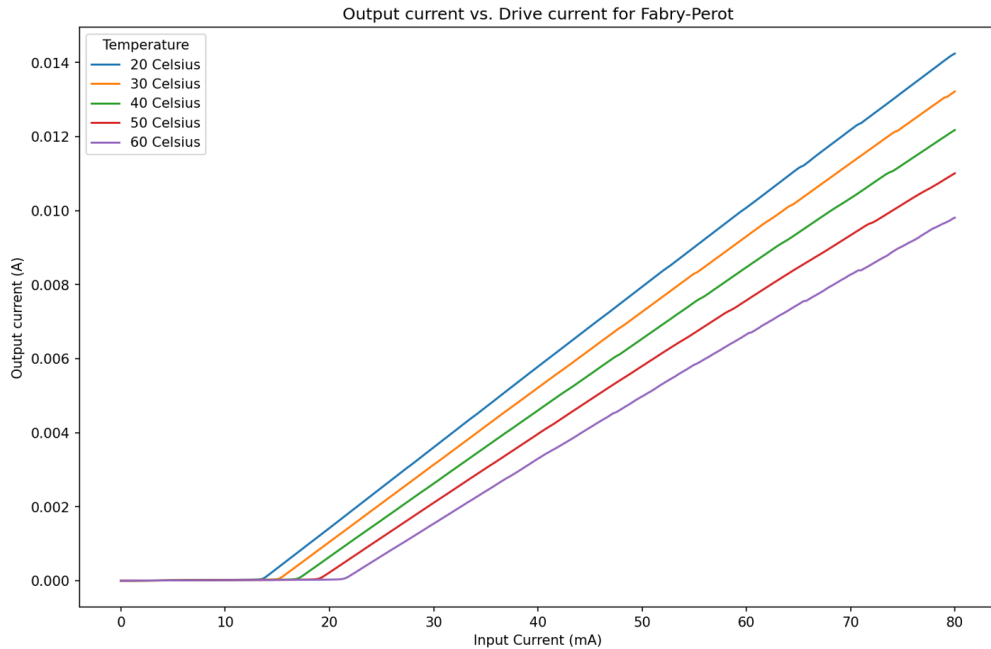


Figure 4.11: LI curves of a Fabry-Perot cavity operating at 1.5 microns, categorised by temperature.

One set of LI curves were generated for the Fabry-Perot device, over a range of 20-60 degrees celsius. There was a very clear decrease in slope efficiency and increase in threshold current with increases in temperature.

4.3.2 Single-Mode Laser

Figures 4.12, 4.13, and 4.16 contain the LI curves, corresponding threshold currents versus temperature, and slope efficiencies versus temperature for the 700 micron single-mode laser. Figures 4.14 and 4.15 are simulations generated by the Python script.

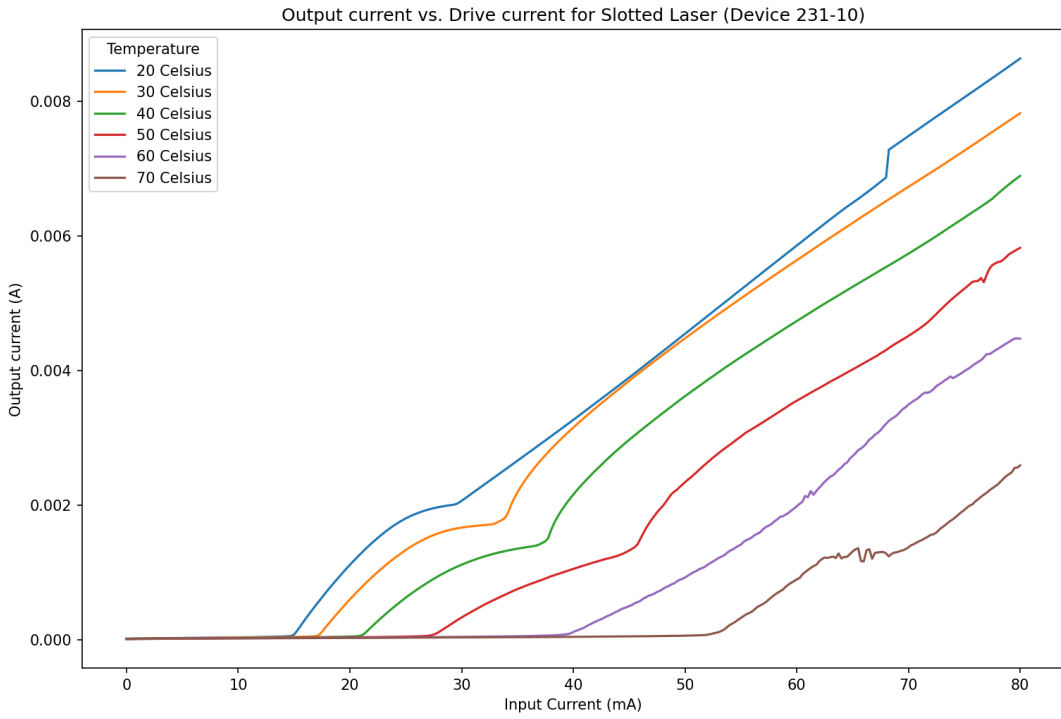


Figure 4.12: LI curves corresponding to different temperatures, generated by the 700 micron single-mode laser.

The LI curves generated by the single-mode laser demonstrated a similar trend vs temperature as that seen for the Fabry-Perot cavity. An increase in threshold current, and a decrease in the slope efficiency.

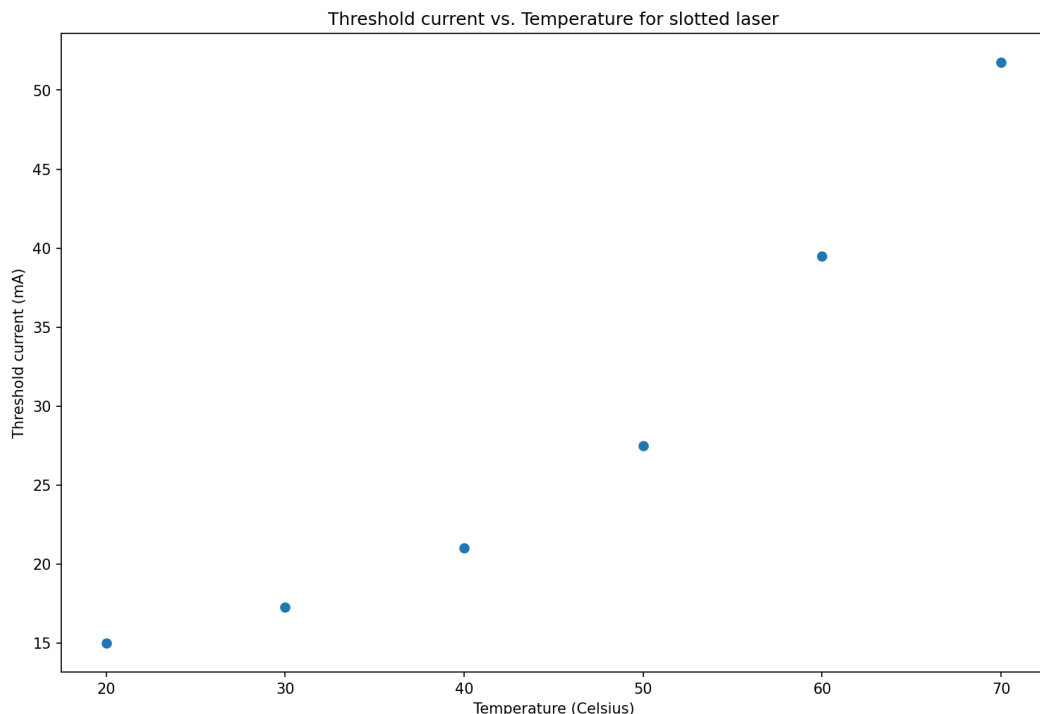


Figure 4.13: Threshold current vs. Temperature for the 700 micron single-mode laser.

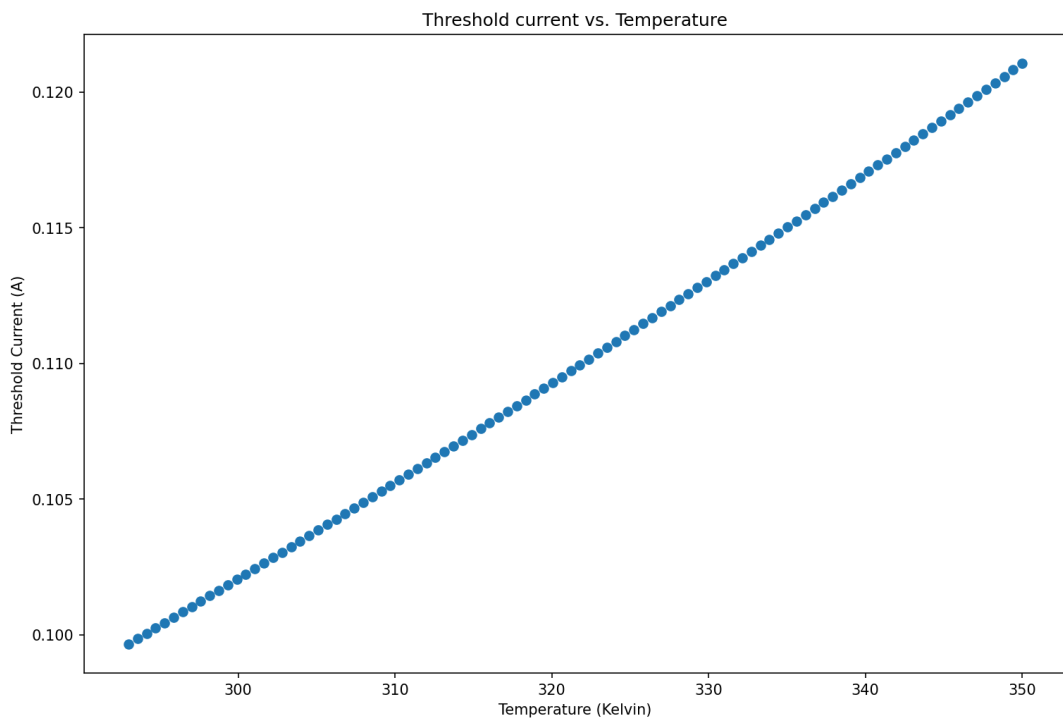


Figure 4.14: Simulated threshold current vs. temperature. A shallower, but similarly shaped curve was generated for the relationship.

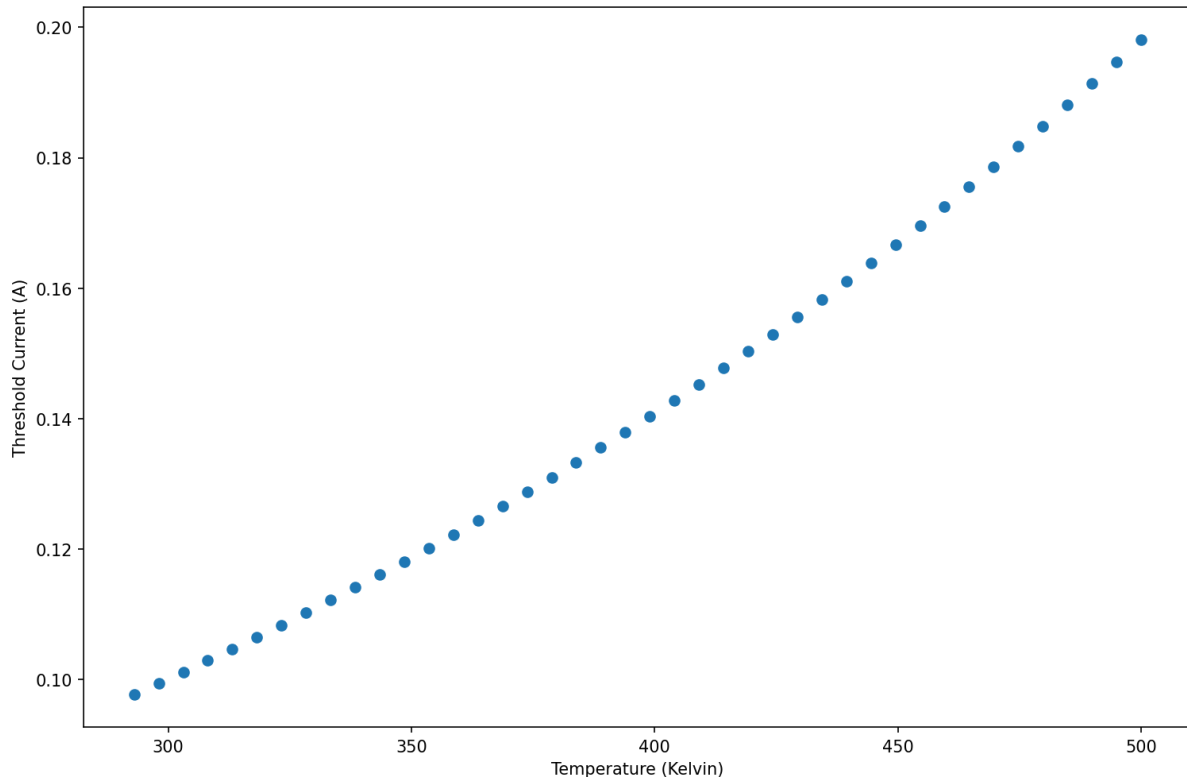


Figure 4.15: Another simulation, run with different parameters and constants, demonstrates the curve more distinctly.

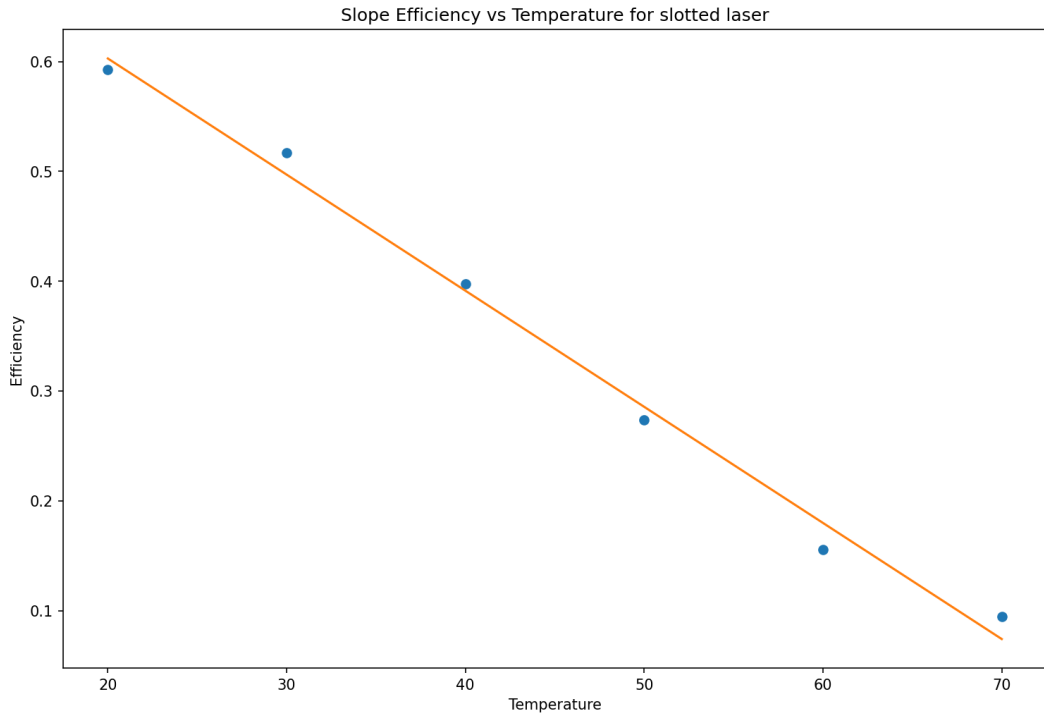
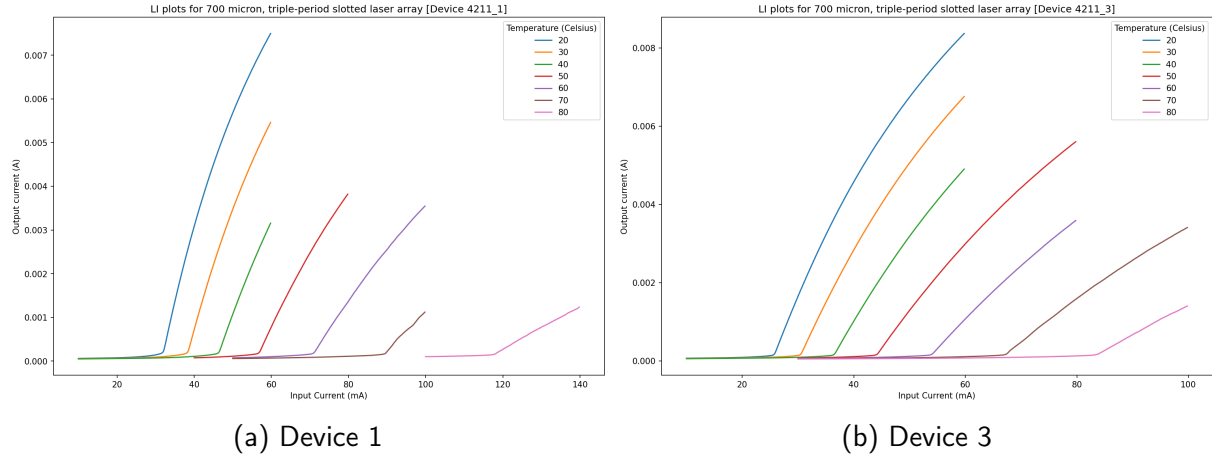


Figure 4.16: Slope efficiency vs. Temperature for the 700 micron single-mode laser.

The exponential trend of the threshold current with increasing temperature was consistent with results that were simulated. There was a dramatic decrease in the threshold current of the laser with increases in temperature, as expected. The simulation was inaccurate in the details of real values and the steepness of the curve due to the lack of simulation of the grating section, but provided a shape that could be expected of the relationship between the threshold current and temperature, and that shape was observed.

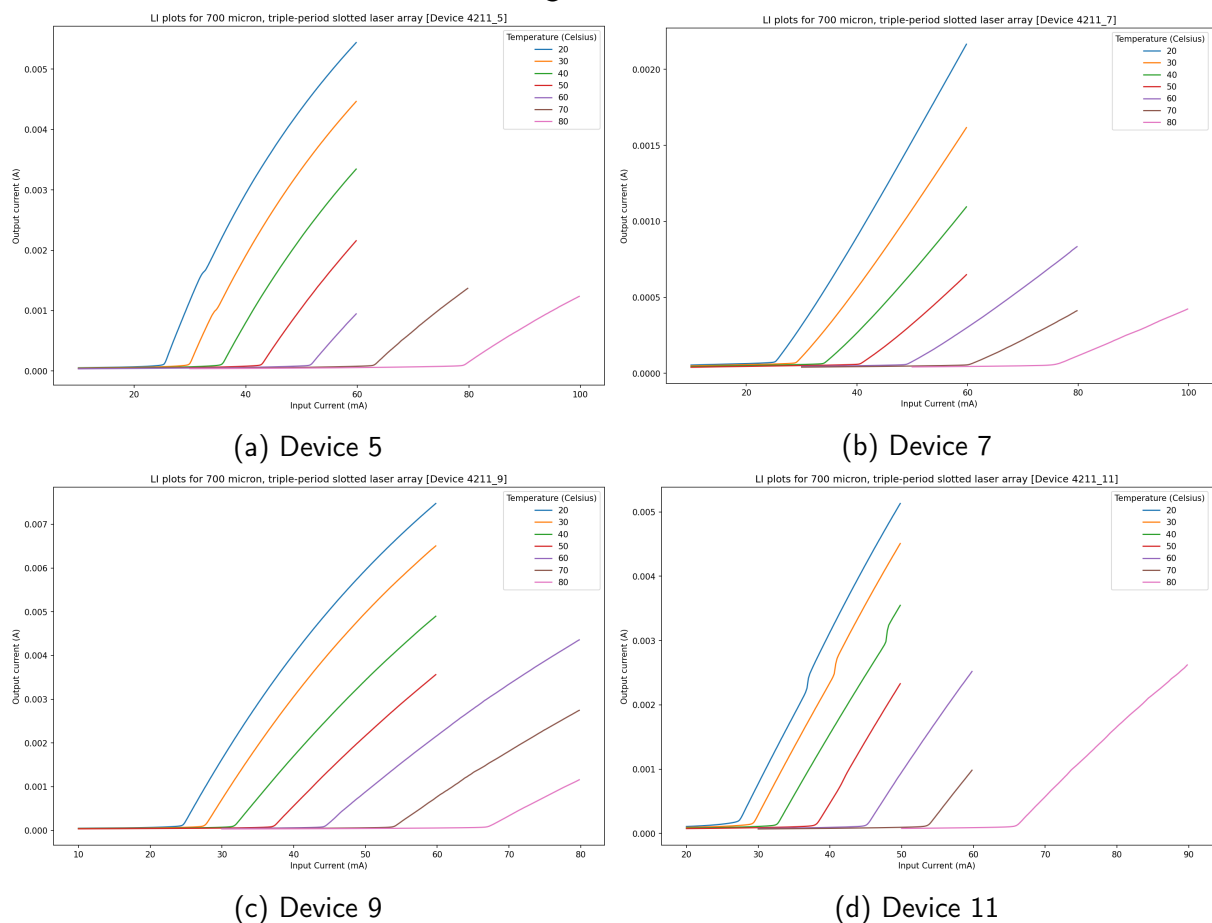
Figure 4.18 contains LI curves for 6 single-mode, 700 micron devices from a single laser array. The trend of lower slope efficiencies and higher threshold currents with increased temperature is clearly visible from the LI curve of each device.



(a) Device 1

(b) Device 3

Figure 4.17: .



(a) Device 5

(b) Device 7

(c) Device 9

(d) Device 11

Figure 4.18: Combined LI curves taken from the 700 micron single-mode laser array, categorised by temperature.

4.3.3 Vernier Laser

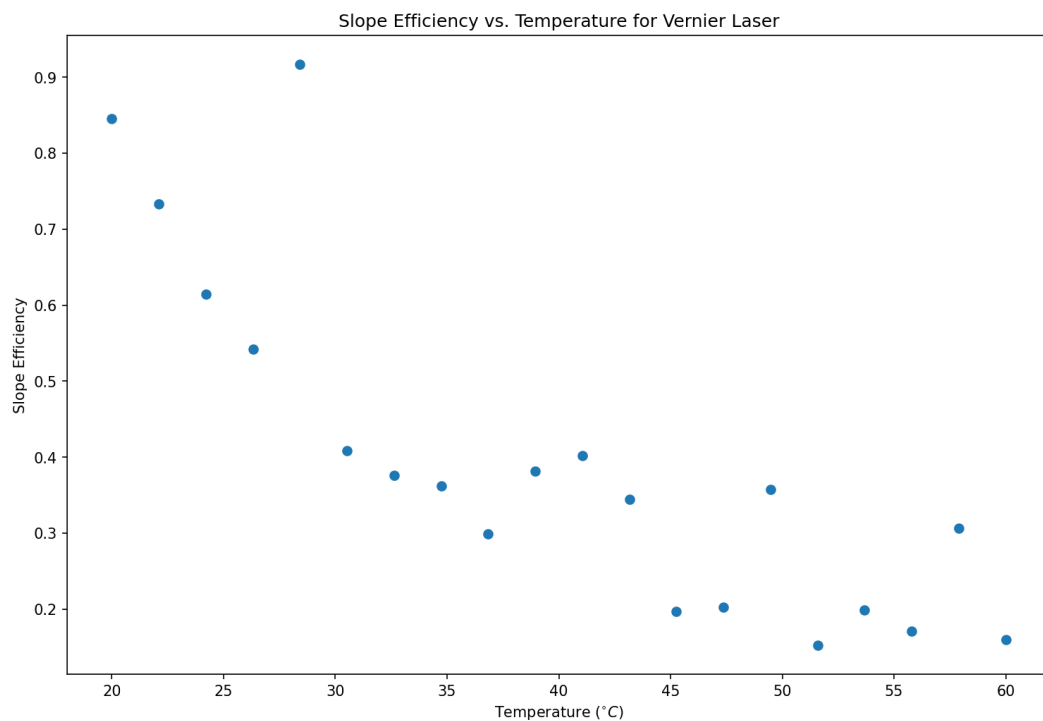


Figure 4.19: Slope efficiency of the Vernier device vs. temperature.

The slope efficiency values for the LI curves taken for the Vernier device showed a general decrease with increased temperature. Threshold current was recorded, but data was too noisy and incomprehensible to make any observations about its relationship with temperature.

4.4 Athermalisation

4.4.1 Fabry-Perot cavity

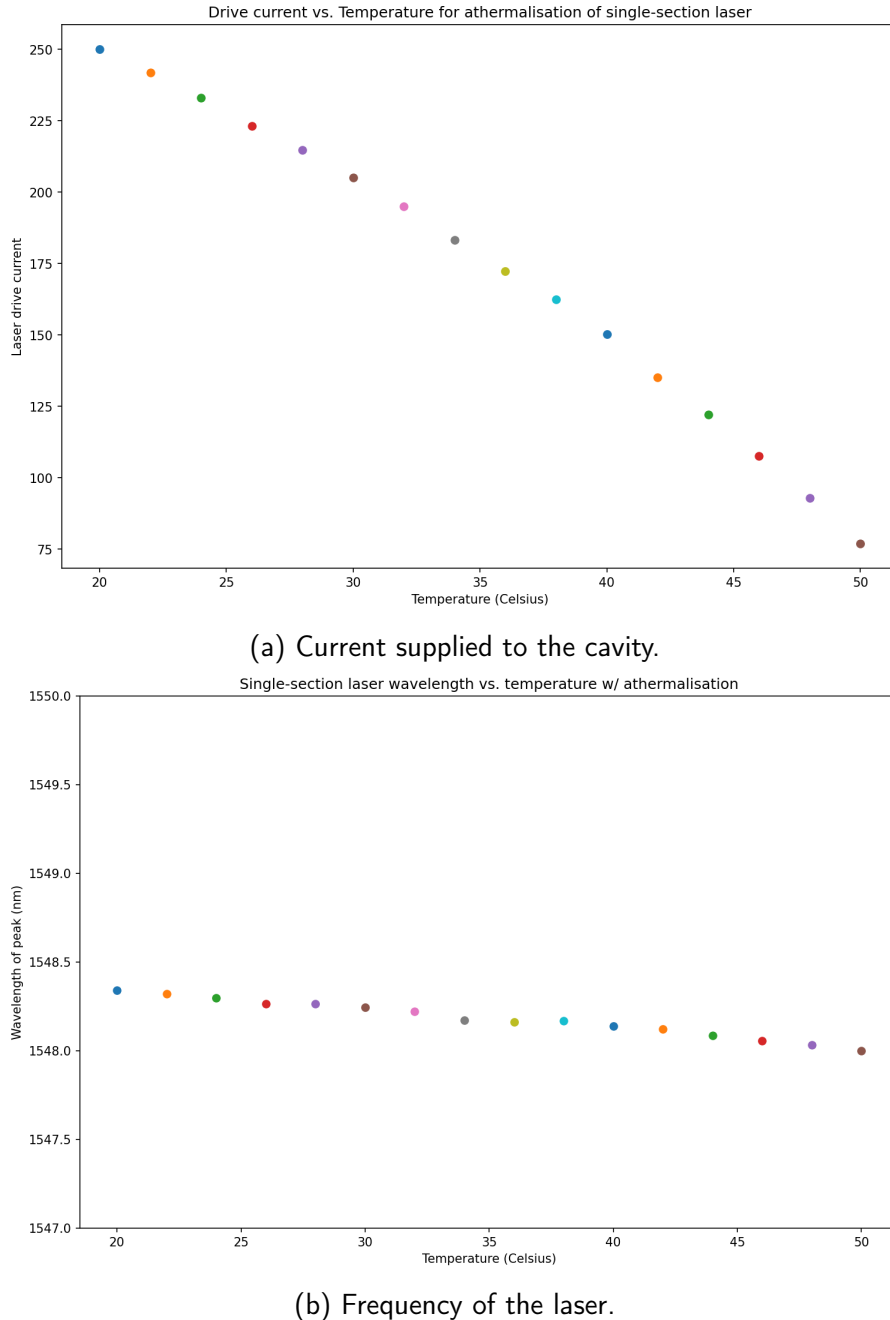


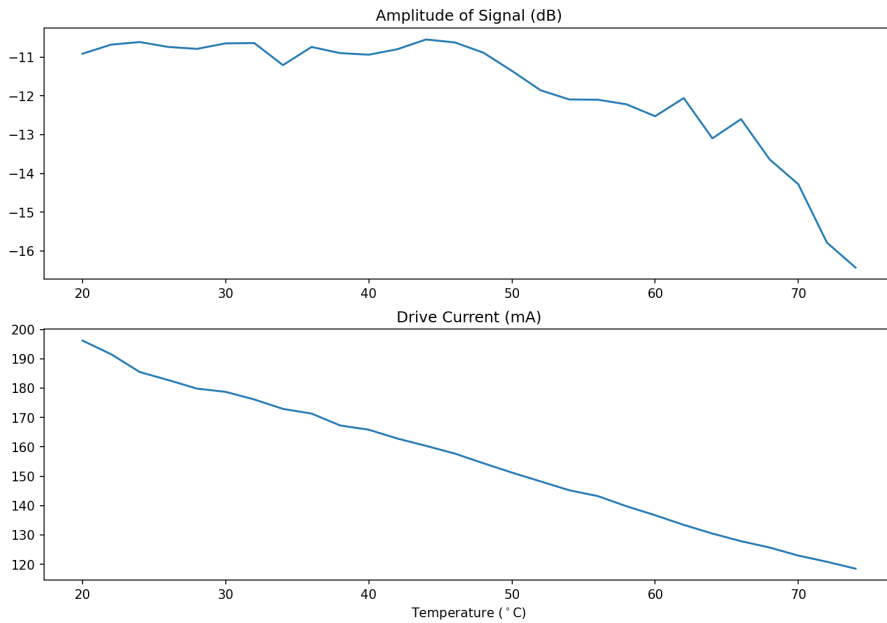
Figure 4.20: Data relating to the athermalisation of the 700 micron Fabry-Perot cavity.

The Fabry-Perot device alone was easily maintained within an acceptable range of the initial wavelength. There was a gradual decrease in the current which allowed the wavelength to be consistent, with manual re-tuning as the temperature was increased in increments of 2°C . This relatively very consistent linear wavelength progression was the most successful of the

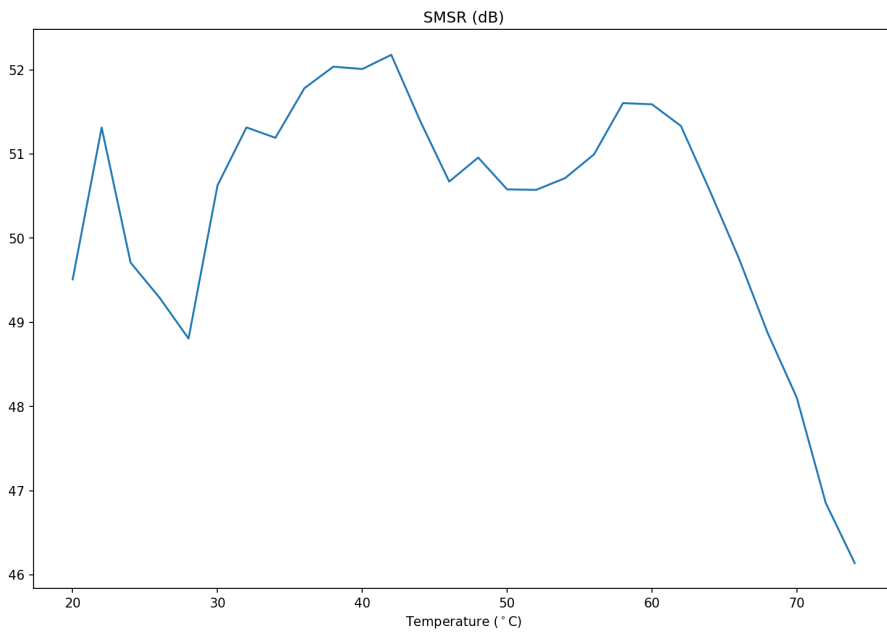
laser devices investigated, however, the range of the wavelength of the laser during its operation was wider than those measured for Vernier device.

The trend in the required change in drive current to maintain the wavelength of the device does not appear as linear, however this tuning was done manually, and a similar but significantly less pronounced non-linear trend is visible in the wavelength of the device over the temperature range. This may have been a result of improper wait times between heating, or simply a result of the manual operation of the re-tuning apparatus.

4.4.2 Single-Mode Laser



(a) Top: Amplitude of the signal, Bottom: Current supplied to the device.



(b) SMSR of the single-mode spectra.

Figure 4.21: Data relating to the athermalisation of the 700 micron single-mode laser.

The single-mode laser was manually re-tuned and maintained at a wavelength of 1.5 microns during the athermalisation tests. There was a relatively linear, shallow decrease in current required to maintain the wavelength, and both the power of the signal and the SMSR of the spectrum peaks were maintained to a reasonable degree until $\sim 60^{\circ}\text{C}$, when both began to drop substantially. Approaching 70°C the relevant spectrum peak became insignificant.

The single-mode device can be said to have achieved useful athermal operation in the range 20°C to 60°C , where the relevant properties of the spectrum to a consistently clear signal are sufficient.

4.4.3 Vernier Laser

The following figures 4.22, 4.23 and 4.24 contain the data corresponding to the athermalisation attempts with the Vernier device.

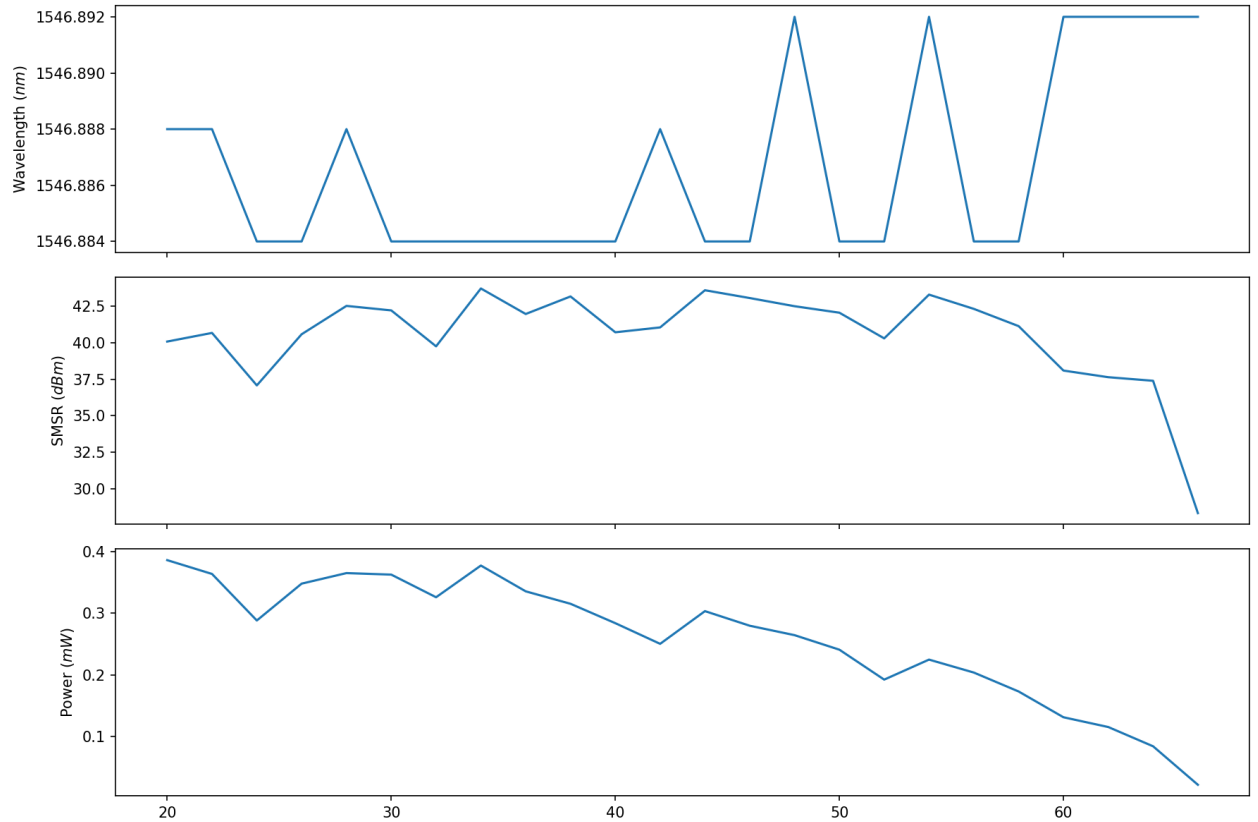


Figure 4.22: Data from first quasi-continuous tuning of the Vernier laser, at 1546.888 nm initial wavelength - temperature, in Celsius, along x-axis.

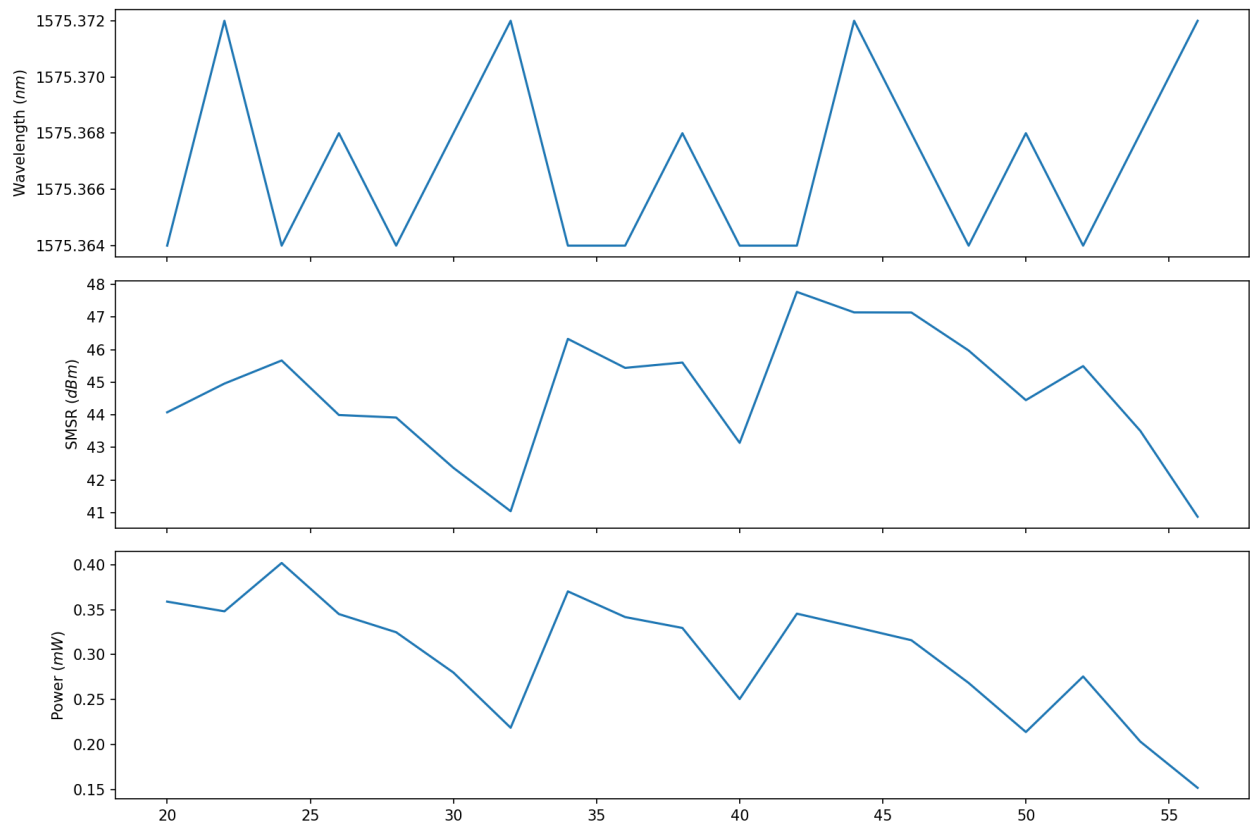


Figure 4.23: Data from second quasi-continuous tuning of the Vernier laser, at 1575.364 nm initial wavelength.

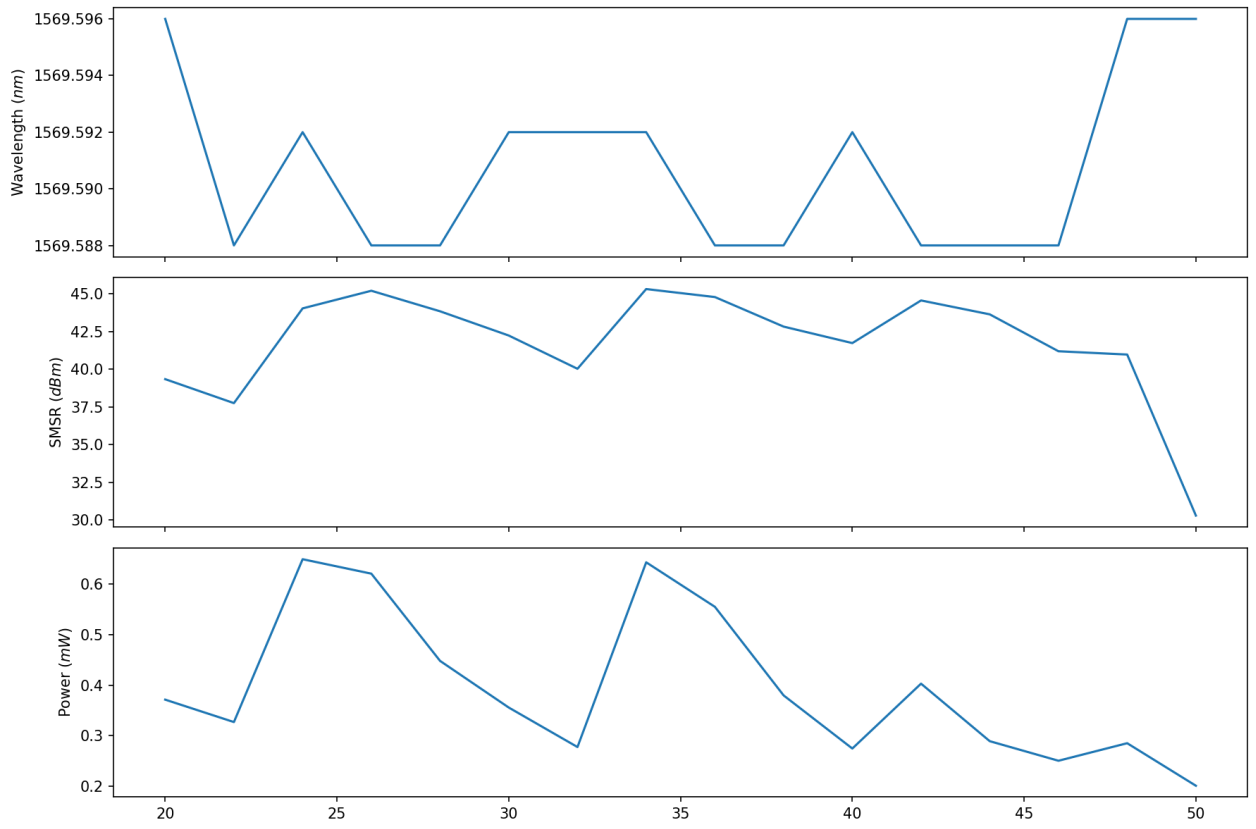


Figure 4.24: Data from third quasi-continuous tuning of the Vernier laser, at 1569.596 nm initial wavelength.

The athermalisation of the Vernier laser was undertaken along 3 different modal pathways, as visible in the tuning map of the laser shown in figure X. The three attempts began at wavelengths of 1546.888 nm, 1575.364 nm, and 1569.596 nm. The first run kept the laser within 0.004 nm of its initial wavelength, the second and third runs maintained a wavelength within a 0.008 nm range of their initial wavelengths.

As the temperature increases, the position of the modes on the tuning map shift, and the SMSR dips as the laser operates closer to the boundary between super-modes. Lower SMSR indicates that another mode has begun lasing and the laser is about to shift to that mode. The dips in SMSR occurred as a result of the laser reaching this boundary during operation. The power of the laser similarly experiences dips at these points.

5 Conclusions

The manual tuning of the laser technologies analysed, as a method of athermalisation is effective within a reasonable range of temperatures ($20\text{-}50/60^\circ\text{C}$) for the wavelengths these tests were conducted with. The drift in wavelength when the lasers are manually re-tuned with reasonable diligence appears within requirements for operation as part of communications infrastructure, specifically in systems where multiple, narrow bands must be run simultaneously.

As none of the experiments dealt with lasers operating lower than room temperature (20°C), this analysis has not been sufficient to confidently claim that the methods used would function as well for lower temperatures. However, with the addition of other, passive heat-conserving technology for the operation of lasers where temperatures may occasionally vary lower than those tested, such a method can fulfill the aim of maintaining consistent operation.

Specifically, the SMSR values of each device during athermalisation experiments was generally favourable within the specified temperature range, with insignificant noise within this range.

The wavelengths were consistent; with all runs demonstrating a wavelength range within 0.08 nm or less of the starting wavelength with the most accurate, Vernier device.

Bibliography

- [1] L.A. Coldren, S.W. Corzine, and M.L. Mashanovitch. *Diode Lasers and Photonic Integrated Circuits. Wiley Series in Microwave and Optical Engineering.* Wiley, 2011.
- [2] B. R. Bennett, R. A. Soref, and J. A. Del Alamo. *Carrier-Induced Change in Refractive Index of InP, GaAs, and InGaAsP,” IEEE Journal of Quantum Electronics, vol. 26, no. 1, pp. 113–122, 1990.*
- [3] M. Cardona and R. K. Kremer “Temperature dependence of the electronic gaps of semiconductors,” in *Thin Solid Films, vol. 571, pp. 680–683, Elsevier, nov 2014.*
- [4] H. Ishii, H. Tanobe, F. Kano, Y. Tohmori, Y. Kondo, and Y. Yoshikuni. “Quasicontinuous wavelength tuning in super-structure-grating (SSG) DBR lasers”, *IEEE Journal of Quantum Electronics, vol. 32, pp. 433–440, mar 1996.*

A1 Appendix

```
44 IE = 0.85 #Current injection efficiency
45 ntr = 1.75*10**18 #Transparency carrier density
46
47 EffMirrorLoss = (1/L)*(np.log(1/(math.sqrt(R1*R2))))
48
49 OutCouplingEfficiency = (EffMirrorLoss)/(EffMirrorLoss + WaveModalLoss)
50
51 #Photon lifetime in cavity
52 PLT = 1/(WaveGroupVel*(WaveModalLoss+EffMirrorLoss))
53
54 ThresholdGain = 1/(Conf*WaveGroupVel*PLT)
55
56 ThresholdCarrier = (ntr)*(math.exp(ThresholdGain/g0))
57 print ('Threshold carrier density:', ThresholdCarrier, 'cm^-3')
58
59 nthr = ThresholdCarrier
60
61 A = nthr
62 BN2 = B*(nthr**2)
63 CN3 = C*(nthr**3)
64 D = A+BN2+CN3
65
66 print (D)
67
68 ThresholdCurrent = (D*Va*q)/(IE)
69 print ('Threshold current:', ThresholdCurrent, 'A')
70
71
72
73 Planck = 6.626*10**-34
74 hbar = Planck/(2*(math.pi))
75
76
77 lamda = 1.5*10**-4 #cm
78 freq = c/lamda*3.4
79
80 '''omega = 2*math.pi*freq #omega associated with frequency'''
81
82
83
```

Figure A1.1: Python code used to generate the simulated non-temperature-dependent LI curves.

```

73
74 Planck = 6.626*10**-34
75 hbar = Planck/(2*(math.pi))
76
77
78 lamda = 1.5*10**-4 #cm
79 freq = c/lamda*3.4
80
81 '''omega = 2*math.pi*freq  #omega associated with frequency'''
82
83
84 I = np.linspace(0, 0.25, 100) #Range of input currents
85
86
87
88 SE = OutCouplingEfficiency*IE*hbar*freq/q #Slope efficiency
89 print('Slope efficiency:', SE)
90
91
92 print('Output coupling efficiency: ', OutCouplingEfficiency)
93
94
95 print('Threshold Gain: ', ThresholdGain)
96
97 output = []
98 for i in range(len(I)):
99     power = SE * (I[i] - ThresholdCurrent)
100    output.append(power)
101
102
103 plt.plot(I, output)
104 plt.ylim(0, 0.025)
105 plt.xlim(0, 0.125)
106 plt.ylabel('Output Power (W)')
107 plt.xlabel('Drive Current (A)')
108 plt.show()
109
110
111
112

```

Figure A1.2: Python code used to generate the simulated non-temperature-dependent LI curves.

```

IThresholdTemp = ThresholdCurrent*(math.exp(T/T0)) #The temperature-dependent threshold current
Planck = 6.626*10**-34
hbar = Planck/(2*(math.pi))

lamda = 1.5*10**-4 #cm
freq = c/lamda*3.4

'''omega = 2*math.pi*freq  #omega associated with frequency'''

I = np.linspace(0, 0.100, 100) #Range of input currents

SE = OutCouplingEfficiency*IE*hbar*freq/q #Slope efficiency
print('Slope efficiency:', SE)

print('Output coupling efficiency: ', OutCouplingEfficiency)

print('Threshold Gain: ', ThresholdGain)

Trange = np.linspace(T0, 350, 100) #Range of temperatures

#calculating the temperature-dependent threshold current
Tthreshold=[]
for i in Trange:

    TempThreshold = ThresholdCurrent*(math.exp(i/T0))
    Tthreshold.append(TempThreshold)

#plotting threshold vs temperature
plt.plot(Trange, Tthreshold, 'o')
plt.xlabel('Temperature (Kelvin)')
plt.ylabel('Threshold Current (A)')
plt.title('Threshold current vs. Temperature')
plt.show()

```

Figure A1.3: Python code used to generate temperature-dependent laser parameters.